PHILIPPE LAMOTHE

A CRUSTAL DEFORMATION STUDY OF THE CHARLEVOIX SEISMIC ZONE IN QUEBEC

Mémoire présenté
à la Faculté des études supérieures de l'Université Laval
dans le cadre du programme de maîtrise en sciences géomatiques
pour l'obtention du grade de Maître ès sciences (M.Sc.)

FACULTÉ DE FORESTERIE ET DE GÉOMATIQUE
UNIVERSITÉ LAVAL
QUÉBEC

Novembre 2007

Abstract

The present research concerns the use of first order spirit levelling and high precision GPS measurements to quantify the local deformations caused mainly by postglacial rebound in the Charlevoix seismic zone, the region with the highest concentrated seismic activity in eastern Canada. For the levelling, part of the Canadian first order network, measured from 1909 to 1991, is analyzed for repeating levelling lines. For GPS, a part of a first order geodetic network along the Saint Lawrence was surveyed by GPS in 1991 and 2005. The coordinate changes of these geodetic points allows for the determination of horizontal and vertical velocities leading to information on the crustal deformation of this region. The results obtained agree quite well with previous GPS surveys conducted on Canadian Base Network (CBN) pillars in eastern Canada and also with geophysical postglacial rebound (PGR) models.

Résumé

La présente recherche porte sur l'utilisation de données de nivellement géométrique de premier ordre et de données GPS de haute précision pour quantifier les déformations locales causées principalement par le rebond postglaciaire dans la zone sismique de Charlevoix, la région de l'Est du Canada avec l'activité sismique la plus élevée. Pour le nivellement, une partie du réseau canadien de premier ordre, mesuré entre 1909 et 1991, est analysée pour des lignes de nivellement mesurées plus d'une fois. Pour le GPS, un réseau de points géodésiques de premier ordre le long du fleuve Saint-Laurent a été remesuré par GPS en 1991 et en 2005. Le changement des coordonnées de ces points géodésiques permet de déterminer les vitesses horizontales et verticales et d'en tirer de l'information sur la déformation de la croûte terrestre dans cette région. Les résultats obtenus sont en accord avec les résultats de précédents levés GPS sur les piliers du Canadian Base Network (CBN) dans l'Est du Canada ainsi qu'avec les modèles géophysiques de rebond postglaciaire.

Foreword

First and foremost, I would like to thank my advisor, Rock Santerre, and my co-advisor, Marc Cocard, for their constant support and availability. A thank you also goes to Stéphane Mazzotti for his support during the GPS data processing. The financial support from the Natural Sciences and Engineering Research Council (NSERC) through my advisor is also appreciated.

I would like to thank my two brothers, Serge and Éric, and my mother, Darquise, whose constant love and strength has been inspirational. A huge thank you goes to my girlfriend, Lianne Dorais, for her unending encouragement and patience with me throughout this whole process. Her love and devotion keeps me going, and persevering. I also cannot leave out the GPS group of the CRG. Never forgotten will be the good times with Simon Banville, Valérie Kirouac, and Stéphanie Bourgon in and outside the GPS lab. This also marks the end of my student days. For this, I would also like to acknowledge my friends out there with which I did my bachelor's degree at York University in Toronto, including Andre Pant, Michael Ilnicki, Alex Ho, Cale Ettenberg, Marie Poulin, and Sylvie Gosselin. A final thank you goes towards my friends out in Ottawa. Simon Patenaude, Lea Barber, Nathalie Hogarth, François Jacques, and everyone else who have been there with me through it all since high school.

In the past two years, I have learned that people, especially myself, are not perfect. What makes us who we are is with whom we share our hopes, dreams, disappointments, and ultimately our triumphs. We spend too much time looking towards the future to appreciate what we, and all those around us, have accomplished. I only hope I do not forget this, long after this page has turned.

Contents

List of Tables

List of Figures

Chapter 1

Introduction

1.1 Context

It is the dynamics of the tectonic plates that provoke earthquakes at their boundaries. Major tectonic activity is most regularly attributed to the release of the strain that accumulates due to the interaction of the plate boundaries. What makes the Charlevoix Seismic Zone (CSZ), located northeast of Quebec City along the Saint Lawrence river, tectonically interesting is the fact that it is not located along one of these plate boundaries. Situated on the North American Plate, the CSZ has had, nevertheless, an important tectonic history.

The CSZ, in Quebec, has the highest recorded frequency of major earthquakes in eastern Canada. The region counts at least 5 earthquakes with a magnitude of 6 or higher on the moment magnitude scale since the 1600's. Different reasons for this high intraplate tectonic activity have been proposed. The first of these is the devonian meteoric impact located in the Charlevoix seismic region [Rondot (1968)] which occurred 350 million years ago. The second is thought to be related to the reactivation of Iapetan normal faults during the Jurassic rifting and opening of the North Atlantic Ocean [Lemieux et al. (2003)]. The third results from the behavior of the crust due to postglacial rebound (PGR), also termed glacial isostatic adjustment (GIA), which is a consequence of the last ice age in the late Pleistocene era 18000 years ago [Mazzotti

et al. (2005)].

Since the early 1970's, there is ongoing monitoring of earthquake activity in the CSZ. Various researchers and institutions, including the Earth Physics Branch (now a part of Geological Survey of Canada), undertook geophysical studies for earthquake prediction using seismology, gravimetry and levelling surveys [Buchbinder et al. (1988)]. The advent of the Global Positioning System (GPS) in the early 1990's, a satellite positioning system conceived as a ranging system from known positions of satellites in space to unknown positions on land, at sea, in air, and space allowed for a cheaper and more accurate method of monitoring crustal deformation on a global level. In 1991, the Geodetic Survey Division (GSD) undertook a high precision GPS campaign using geodetic receivers in the CSZ. Then, in 2003, Natural Resources Canada (NRCan) started a new program to study the geodynamic aspects of earthquake hazard in eastern Canada. The year 2005 thus saw a second high precision GPS campaign undertaken, remeasuring the 1991 geodetic points as well as expanding the study area and the number of sites, including Canadian Base Network (CBN) sites.

Also, part of the first order levelling network with measurements dating back to 1904 [Véronneau et al. (2006)] runs through the CSZ and outlying areas. Levelling has a high measurement accuracy, at the millimeter level. However, due to the advent of geoid modelling as an alternative for vertical datum definition as a result of high costs of levelling, very little has been done since 2001.

1.2 Nature of the problem

Unlike plate boundaries, where seismic activity is directly correlated with plate interactions, the driving mechanisms for intraplate earthquakes are more difficult to determine. In Henton et al. (2006), it is stated that at plate margins, the relative horizontal and vertical velocities are typically of the order of 5-50 mm/yr, which can be resolved with campaign GPS data acquired every year or two over a three to five year period. However, the relative velocities across tectonically stable regions, such as the Charlevoix intraplate environment, are of the order of 1 mm/yr in the horizontal direction, which

is at the current limit of GPS resolution. Similar studies ongoing in the New Madrid intraplate seismic zone, located in the central United States, have also shown that the current strain rates in regions of past large earthquakes is at or below the resolution of geodetic techniques [Kenner and Segall (2000)].

GPS is a powerful measurement technique, but has its limitations, which are caused by many factors. These include errors caused by satellite and receiver clock biases, the troposphere, the ionosphere, the satellite ephemerides, the phase ambiguities, antenna phase center variations, earth tides, ocean loading, and multipath. Errors such as satellite clock biases and ionospheric delay can be eliminated or greatly reduced using specific processing techniques, such as double differencing. Other errors, such as tropospheric delay and antenna phase center variations, can be eliminated through the use of modelling of the pertaining effect. A large number of observations over a long period of time are also necessary to correctly reduce errors. These do not include gross errors that can be introduced during the collection of the data, such as incorrectly measured antenna heights.

It is therefore important to be able to correctly and optimally process such large GPS data sets while concurrently keeping track of all these factors and their impacts on the final solutions in order to have coherent results. This is especially true for dealing with height coordinates and the vertical velocities of markers derived. It has been shown that errors in the height coordinates are at least twice as high as those for horizontal coordinates, and that there is a strong correlation between the vertical coordinate component and the tropospheric zenith delay [Santerre (1991); Santerre and Beutler (1993)]. Also, the campaign network has to be tied to a stable reference frame, such as the International Terrestrial Reference Frame (ITRF2000) [Altamimi et al. (2002)] in order to facilitate inter-comparison of geodetic solutions and hence geophysical interpretation of crustal motion.

1.3 Objective

The research objective is to quantify the postglacial rebound (PGR) signal in the CSZ using two methods. The first is by the determination of vertical velocities from select repeating levelling lines from the first order Canadian network in and around the CSZ. The second is by post processing high precision GPS observations from two different campaigns, in 1991 and 2005, to determine horizontal and vertical velocities of markers in the CSZ. It will then be possible to compare these results with those from a larger GPS survey conducted on Canadian Base Network (CBN) pillars in eastern Canada as well as crustal motions predicted by a PGR model.

1.4 Methodology

The methodology is divided into two sections. The first one will discuss the method in which vertical velocities are derived from the first order levelling network and the second one, the method in which the horizontal and vertical velocities are obtained from the GPS campaigns.

1.4.1 Spirit levelling

The levelling lines of the first order Canadian network used to define the Canadian Geodetic Vertical Datum (CGBD28) were repeatedly measured during different surveying years. This means that the data collection occurs along the same benchmarks every year that it is remeasured. It is thus possible to compare the relative geopotential difference, which are related to orthometric height differences, of the same markers in independent levelling lines and determine the relative vertical motion of the sites. MATLAB subroutines were developed to match markers from different years of independant levelling lines and to cumulate the geopotential differences along the surveyed line.

It is then possible to calculate the vertical velocity of the markers of the levelling lines in order to obtain the relative vertical motion, in mm/yr. This is done by first subtracting the relative geopotential differences between the two years and dividing it by the number of years elapsed between the surveys. Then, these geopotential differences are converted into mm/yr using the gravity values measured at the benchmark. The velocity variation of the markers between the beginning and the end of the levelling line will be compared with the variation of velocity between GPS sites derived from previous GPS campaigns on CBN sites and the uplift velocities predicted by PGR models.

1.4.2 GPS technique

The first part of the methodology for post processing high precision GPS campaign data concerns network design and the data collection strategy. The GPS stations encompass the region of seismicity of the CSZ to maximize spatial resolution, with an equal number of first order geodetic markers on both sides of the Saint Lawrence river directly parallel on the north and south shore. The measurements are then taken for long sessions, usually lasting two to three days on the geodetic markers, which have clear sky visibility in unpopulated areas to minimize human tampering. This is the case for a GPS campaign undertaken by the Geodetic Survey Division (GSD) in 1991 which was remeasured in 2005. It will henceforth be referred to as the Charlevoix network.

In the second part, the GPS data from both the 1991 campaign and the 2005 campaign is processed with the BERNESE v5.0 software [Hugentobler et al. (2004)]. It is a high performance and high accuracy GPS post processing package. Some of its characteristics include state of the art modeling, detailed control over all relevant processing options, performant automatization tools, the adherence to up to date internationally adopted standards, and inherent flexibility due to a modular design.

The BERNESE software will be used for tying the Charlevoix network to the ITRF2000. The reference stations for the tie are chosen as a function of their location with respect to the Charlevoix network and will be rigorously constrained to their nominal positions and velocities. These nominal positions and velocities will also be used to tie the two GPS campaigns in time. As for the determination of the velocities of

the Charlevoix network, BERNESE has the modules necessary to compute them using the least-squares technique. The velocities, originally in the ITRF2000 reference frame, are mapped into a stable North America reference using the ITRF2000/North America rotation vector defined in Altamimi et al. (2002). The velocity rotation vectors of the Charlevoix network markers are calculated (using MATLAB subroutines) and are subsequently subtracted from the ITRF2000 reference frame velocities. This will result in relative horizontal velocities of the markers of the Charlevoix network on the stable North American (NOAM) Plate.

The resulting relative velocities on stable NOAM will then be validated by comparing them with previous Canadian Base Network (CBN) GPS campaign horizontal and vertical velocities derived from data collected between 1997 and 2003 in eastern Canada and published by Mazzotti et al. (2005) from the Geological Survey of Canada (GSC). Since the same velocity rotation vector, and the same post processing technique presented in Mazzotti et al. (2003) is used, it is possible to validate the resulting horizontal and vertical velocities calculated in this research. The Charlevoix network horizontal and vertical velocities will also be validated by comparing them to the ICE-3G PGR model of Tushingham and Peltier (1991), which is an independant method used to estimate crustal motion based on geophysical predictions of postglacial relative sea-level variations due to melted ice sheets.

1.5 Research contribution

The only previously published work on crustal monitoring in the Charlevoix region using GPS has results that date back to 1997 [Mazzotti et al. (2005)]. Processing both the 1991 and 2005 data not only gives a longer temporal resolution, but allows for a densification, or increased spatial resolution, of the crustal motion in terms of relative horizontal and vertical velocities derived from GPS in the affected CSZ zone. It will be shown that even with pre IGS era GPS data, it is possible to obtain high precision results with an accuracy of a few millimeters. Consequentially, we have provided evidence that even though the crustal motion is at the resolution limit of GPS, a PGR signal can be distinguished from GPS noise in the vertical direction.

The research will also allow the comparison of the spatial trend of the vertical velocities derived from the Charlevoix GPS network observations with that of relative velocities derived from lines of the Canadian first order levelling network that date back to 1909.

It is also now possible to justify the need for installing more permanent GPS stations in the region as a replacement of campaign GPS data. Permanent stations allow better resolution of short-term (less than one year) deformation episodes, and better estimates of long-term velocities.

1.6 Contents of thesis

After the introductory chapter 1, chapter 2 presents a description of the geophysical and tectonic characteristics of the CSZ, including the postglacial rebound situation in the region and historical earthquakes. Chapter 3 discusses the levelling portion of the investigation, including a description of the data available, the processing strategy and the results obtained from the analysis of the levelling lines repeatability. Chapter 4 describes the conventional processing method for high precision GPS networks, the processing method of the 2005 and 1991 campaigns, and coordinate results of the Charlevoix network derived from the processing. Chapter 5 presents the velocities of the Charlevoix network obtained from the 2005 and 1991 campaign coordinate results. This includes the horizontal velocities in the ITRF2000, the relative horizontal velocities with respect to the stable North American Plate as well as the vertical velocities. Chapter 6 compares the GPS relative horizontal and vertical velocities of chapter 5 and relative vertical velocities of the levelling results of chapter 3 with those of the eastern Canada CBN network as well as with the results of the simulated ICE-3G PGR model of Tushingham and Peltier (1991) from Mazzotti et al. (2005). Chapter 7 elaborates on conclusions and gives perspectives on future work.

There are two appendixes. Appendix A presents tables relating to the data of the GPS campaigns as well as intermediate results of the processing from chapter 4. Appendix B gives a detailed explanation of the link of two of the 1991 and 2005 campaign

sites on Ile aux Coudres and the processing method used to obtain the eccentricity between the two sites.

Chapter 2

Geophysical description of the Charlevoix seismic zone in Quebec

This chapter will present background information on the region of study, that is of Charlevoix in Quebec. The first section will give a brief summary of the geological and tectonic characteristics of the CSZ. The second section will present the postglacial rebound situation in North America and historic earthquakes originating from the CSZ.

2.1 Geological background

The major tectonic plates of the Earth can be seen in Figure 2.1[1]. The CSZ is located on the interior of the North American Plate.

Charlevoix is located on the north shore of the Saint Lawrence river, in the Saint Lawrence valley region, about 100 km northeast of Quebec City. The following geological summary is mainly based on Mazzotti et al. (2005). The earliest tectonic phase is the Grenville orogen, from 1100-900 million years ago. Then the region was affected by the rifting and opening of the Iapetus, or proto Atlantic Ocean around 700-600 million years ago, or during the late Proterozoic. This event corresponds to the formation of

[1] http://pubs.usgs.gov/gip/earthq1/fig1.gif

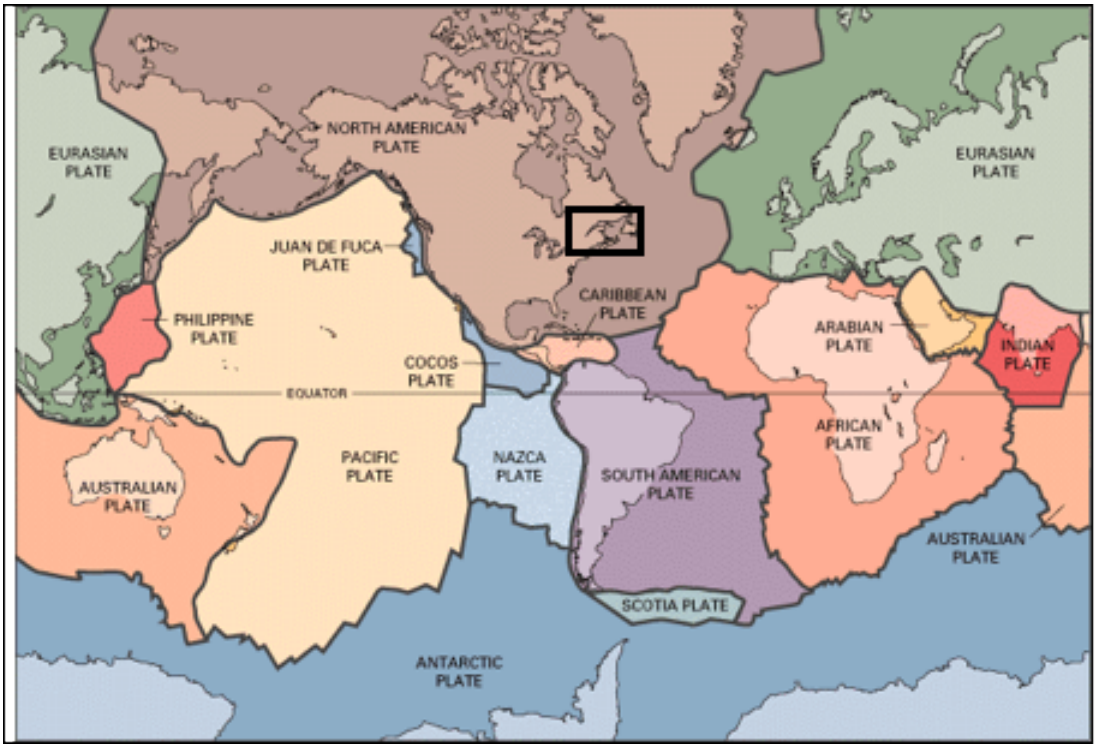

Figure 2.1: Major tectonic plates of the Earth. The black rectangle represents the location of the CSZ

large-scale systems of normal faults. The major structures of the Iapetan system include the Saint Lawrence rifted margin, Ottawa, and the Saguenay grabens in Canada. The closing of the Iapetus Ocean corresponds to different development phases of the Appalachian orogen during the mid to late Paleozoic. The appalachians nappes were thrust over the North America craton as far west as the Saint Lawrence valley. The reactivation of Iapetan normal faults during the Jurassic period, involving the rifting and opening of the North Atlantic Ocean is the last phase of significant tectonic activity in the Saint Lawrence area. Figure 2.2 shows the geological setting of the Saint Lawrence river, where the smaller dotted ellipse is the CSZ, the area of study. The second larger dotted ellipse is the Saint Lawrence seismic zone (LSZ). The major tectonic events represented are the Grenville orogen (∼1100-900 Ma), the Grenville front (long-dash barbed line) marks the boundary between the Grenville province (stripped pattern) and the North America craton; Iapetus ocean opening (∼700-600 Ma), the light gray shading shows the spatial extent of the western Iapetan rifted margin and aulacogens; Appalachian orogen (∼450-250 Ma), the Appalachian front (short-dash barbed line)

marks the western limit of thrust nappes.

The Logan fault is the main structure in a series of thrusts faults that stretches from Lake Champlain in southern Quebec to the Gaspe. It represents a fracture in the Earth's crust. It constitutes the boundary between the Saint Lawrence platform and the Appalachian Orogen. Also called Logan's line, it has been inactive for hundreds of million of years, and follows the Saint Lawrence river, through the CSZ[2].

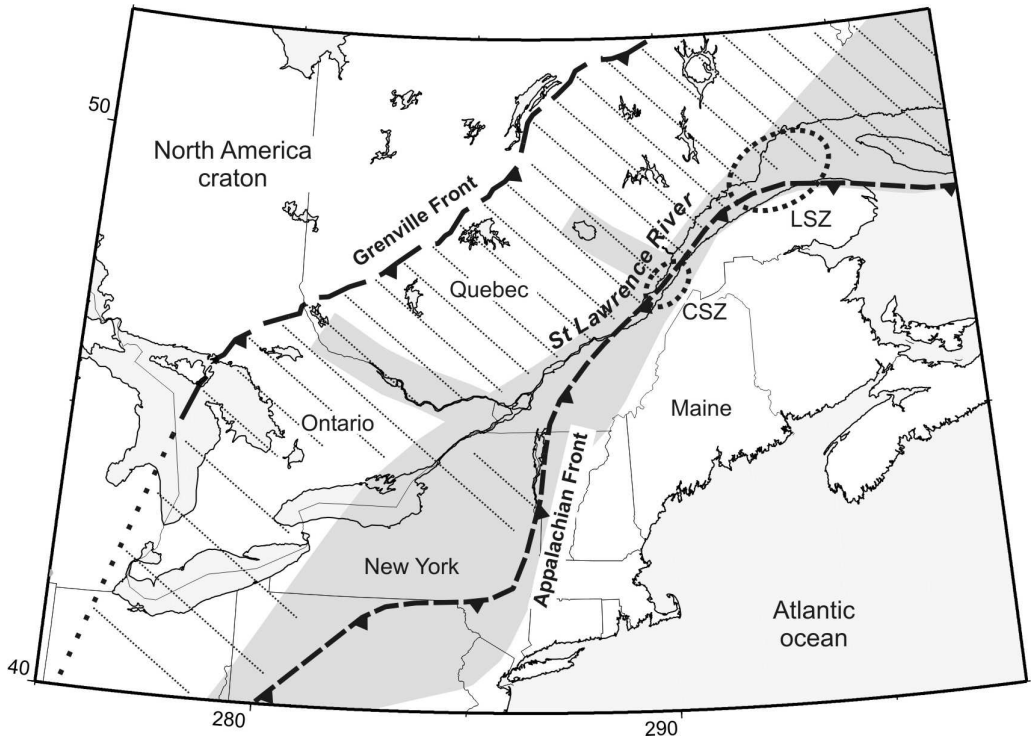

Figure 2.2: Geological setting of the Saint Lawrence valley from Mazzotti et al. (2005)

The tectonic characteristics are further complicated due to a meteorite impact approximately 350 million years ago in the southern part of the CSZ which created a crater with a diameter of 60 km, spanning from Baie-Saint-Paul to La Malbaie [Rondot (1968), Lemieux et al. (2003)]. Also, during the late Pleistocene era, ice covered most of the Quebec-Labrador region which then retreated causing an effect known as postglacial rebound, which will be discussed further in section 2.2.

[2]http://geoscape.nrcan.gc.ca/quebec/upperlower_e.php

2.2 Postglacial rebound

2.2.1 Definition of postglacial rebound

Postglacial rebound (PGR), also called glacial isostatic adjustment (GIA), is the rise of land masses that were depressed by the weight of ice sheets during the ice age cycles, through a process known as isostatic depression. It affects northern Europe, especially Scotland and Scandinavia, Siberia, Canada, the Great Lakes of Canada and the northern United States. At the peak of the last ice age about 18000 years ago, much of northern Europe and Canada was covered by ice sheets up to 3 kilometers thick, including the Quebec-Labrador region, where the CSZ is located [Peltier (1994)]. The weight of the ice caused the crust to sink into the solid viscous mantle. When the glaciers retreated, the removal of the weight from the depressed land led to a rapid uplift due to the buoyancy of crustal material relative to the mantle. Due to the very high viscosity of the mantle, it takes many thousands of years for the land to reach an equilibrium level.

Figure 2.3[3] shows the ice extent and cover during the late Pleistocene era.

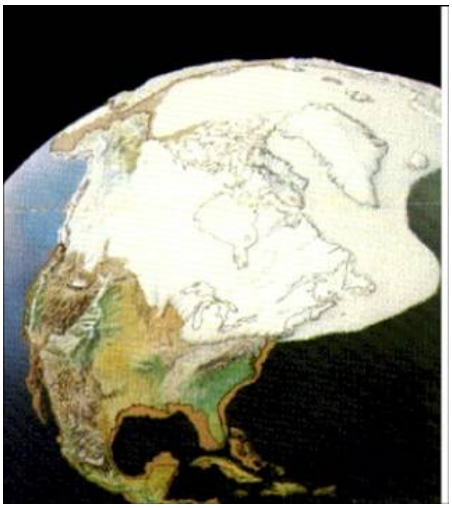

Figure 2.3: Ice covering North America during the late Pleistocene ice age

[3] http://palaeo.gly.bris.ac.uk/Palaeofiles/Pleistocene

2.2.2 Effects of postglacial rebound in the Quebec-Labrador region and the Maritimes

Figure 2.4, taken from Henton et al. (2006), shows PGR derived from regional GPS solutions on CBN points across Canada. The CBN is a national network of high-stability pillar monuments with forced-centering mounts for GPS antennas. For eastern Canada, site of one of the major ice domes of the Laurentide Ice Sheet [Peltier (1994)], the highest uplift rates are in the vicinity of James Bay through to southwestern Labrador. The rates decrease to the south and become negative towards the coastal Atlantic margins. This directional change in vertical uplift indicates the point where subsidence starts occurring, due to mass redistribution after the last ice age [Henton et al. (2006)]. The results from the CBN in Canada have quantified, nationally, the presence of PGR.

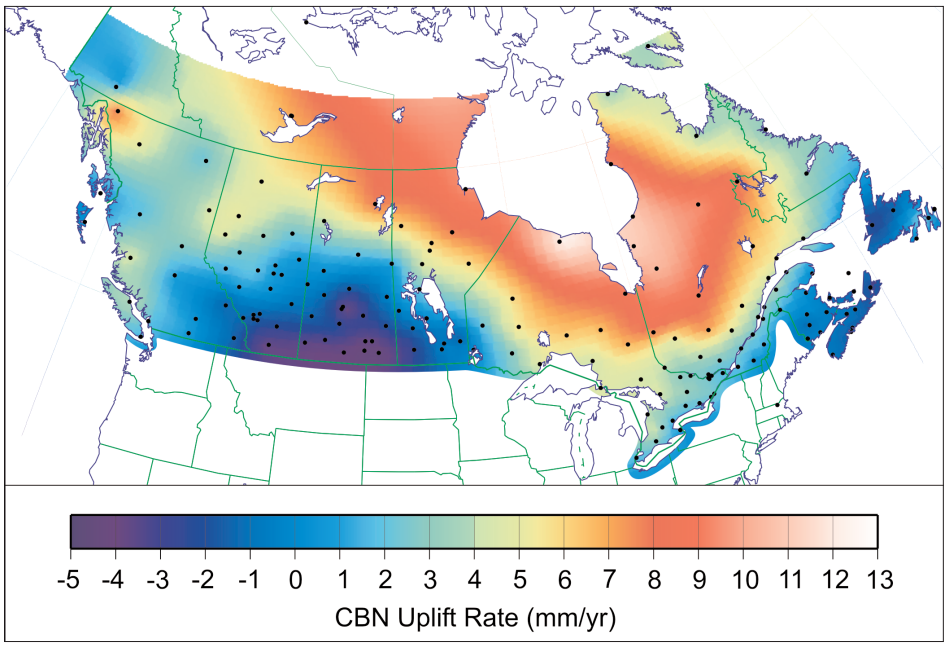

Figure 2.4: Preliminary CBN vertical rates using GPS from Henton et al. (2006)

2.3 Historic earthquakes

The CSZ is abnormally active for an intraplate environment. There have been 5 earthquakes exceeding 6 on the moment magnitude scale in the last 350 years. Figure 2.5[4], taken from Earthquakes Canada shows the major earthquakes (identified with stars) that have had a moment magnitude of 6 or greater. The last major tectonic event in the CSZ was the 1925 Charlevoix earthquake which occurred on February 28, one which had a moment magnitude of 6.2 and was felt more than 1000 km away. It is now known that the earthquake occurred along the section of the Saint Lawrence near Ile aux Lièvres and that its depth was about 10 km beneath the surface[5]. Other important earthquakes were those originating from the Charlevoix/Kamouraska region in 1663, 1791 and 1860 with an estimated magnitude exceeding 6. In the 1900's, another notable earthquake originating from the Saguenay in Chicoutimi occurred in 1988. Although not in the CSZ zone, this earthquake was felt from as far away as Montreal[6].

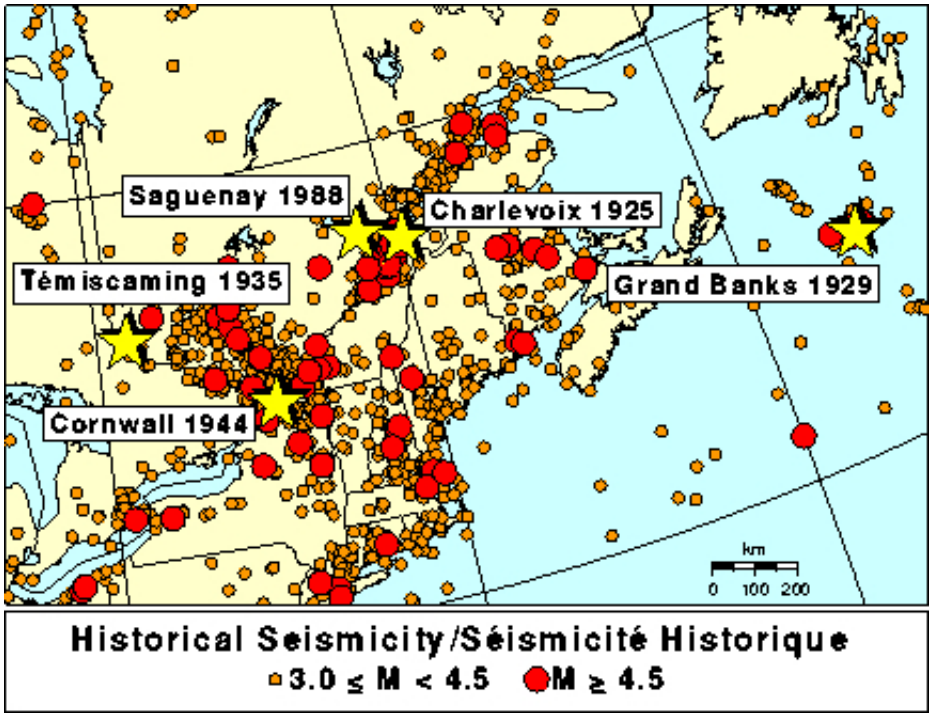

Figure 2.5: Historical seismicity in Charlevoix in Quebec from Earthquakes Canada

[4]http://earthquakescanada.nrcan.gc.ca/historic_eq/20th/e_damaging_e.php#20centdameq
[5]http://earthquakescanada.nrcan.gc.ca/historic_eq/20th/1925/19250301_e.php
[6]http://earthquakescanada.nrcan.gc.ca/historic_eq/20th/saguenay88/saguenay88_e.php

According to Mazzotti et al. (2005), the presence of large earthquakes along the Saint Lawrence valley indicates some level of brittle deformation in the crust. Based on the statistics of a truncated Gutenberg-Richter distribution, the estimated seismic strain rates in most of eastern Canada are about 10^{-13} - 10^{-11} /yr. Exceptions to these low strain rates can be found in the CSZ and LSZ. Earthquakes statistics in these two regions are associated with seismic strain rates of 3-23 x 10^{-9}/yr in CSZ and 0.1 - 5 x 10^{-9} /yr in LSZ.

Chapter 3

Levelling network

In this chapter, the levelling portion investigated will be presented. The first section will give an explanation of levelling, including the relationship between uncorrected differential levelling, orthometric heights and geopotential numbers. The second section will discuss the strategy used to obtain relative geopotential differences of the markers from the levelling lines and the results in the CSZ. The third section will explain how marker velocities can be obtained from geopotential differences, and subsequently the velocity gradient of the levelling lines. Velocity gradient results will then be presented for select levelling lines outside the CSZ.

3.1 Spirit levelling

Levelling is a process by which the geometric height difference along the vertical is transferred from a known benchmark to a forward station [Meyer et al. (2006)]. A levelling line connects two stations A and B as shown in figure 3.2. If the stations are far apart, the levelling section will contain several turning points, the vertical geometric separation between which is denoted as δv_i. δv_i between two points can be measured by the use of two vertical rods set up at each of the two points. The levelling instrument is installed at equal distances between the two rods. Figure 3.1 shows the spirit levelling concept. The height determined by levelling is the sum of the δv_i whereas the ortho-

metric height is the sum of the $\delta H_{B,i}$, which is the vertical geometric separation of the two equipotential surfaces along the plumb line for B. These two are not the same due to the non-parallelism of the equipotential surfaces whose geopotential number values are denoted by C. The geometric separation can be calculated as:

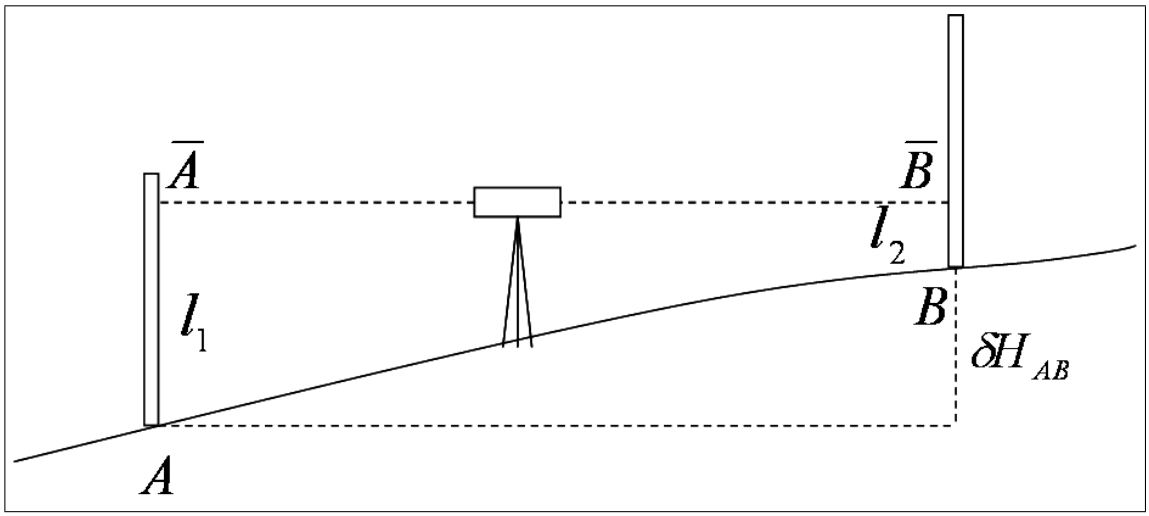

Figure 3.1: Spirit levelling concept from Hoffmann-Wellenhof and Moritz (2005)

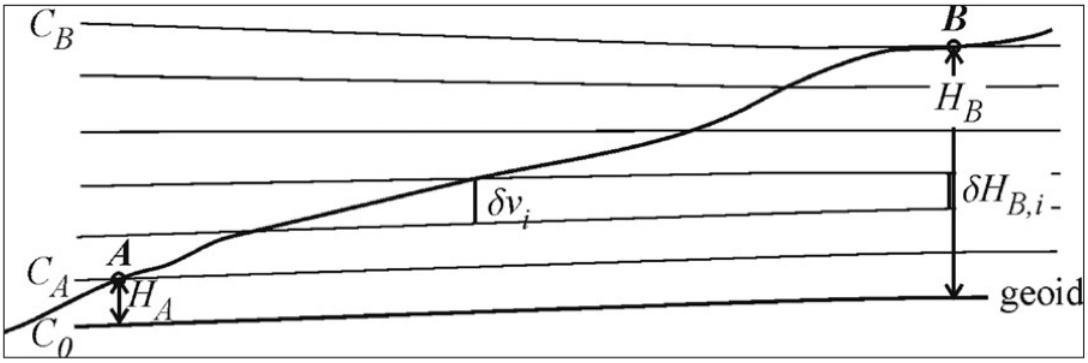

Figure 3.2: Comparison of levelling height differences δv_i with orthometric height differences $\delta H_{B,i}$. From Hoffmann-Wellenhof and Moritz (2005)

$$\delta v_i = l_1 - l_2 \tag{3.1}$$

where $\bar{A}$ and $\bar{B}$ are the height readings on the rods. Point A is known as the backsight and point B as the foresight.

δv_i, the levelling height difference does not generally produce orthometric height differences, $\delta H_{B,i}$. In other words, because $\delta v_i \neq \delta H_{B,i}$, and the orthometric height at B can be written as $H_B = H_A + \sum \delta H_{B,i}$, it follows that $H_A + \sum \delta v_i \neq H_B$.

The orthometric height, H_B, is obtained from the sum of the differential levelling height differences, $\sum \delta v_i$, in the following way. The following is taken mainly from Meyer et al. (2006). Suppose an observed sequence of geometric height differences δv_i has been summed together for the total change in geometric height along a section from station A to B, $\Delta v_{AB} = \sum \delta v_i$. If the change in orthometric height from A to B is denoted as ΔH_{AB}, then a change in orthometric height can be obtained using:

$$\Delta H_{AB} = \Delta v_{AB} + OC_{AB} \tag{3.2}$$

where OC_{AB} is the orthometric correction and has the form of:

$$OC_{AB} = \sum_{A}^{B} \frac{g_i - \gamma_0}{\gamma_0} \delta v_i + \frac{\bar{g}_A - \gamma_0}{\gamma_0} H_A - \frac{\bar{g}_B - \gamma_0}{\gamma_0} H_B \tag{3.3}$$

where:

g_i : observed force of gravity at the observation stations

$\bar{g}_A, \bar{g}_B$: average values of gravity along the plumb lines at A and B

γ_0 : arbitrary constant often taken to be the value of normal gravity at 45°latitude

Finally, geopotential numbers can then be obtained from the orthometric height multiplied by the average acceleration of gravity along the plumb line:

$$C_A = \bar{g}_A H_A \tag{3.4}$$

The gravity measurement is taken into consideration in order to obtain the geopotential number. Geopotential numbers are measured in geopotential units (g.p.u), where:

$$1\,g.p.u = 1\,Kgal\,meter\ = 1000\,gal\,meter = 1\,m\,Kgal \tag{3.5}$$

in which:

$$1\,gal = 0.01\,\frac{m}{s^2} = 1\,\frac{cm}{s^2} \tag{3.6}$$

For example, 9.8 $\frac{m}{s^2}$ = 980 gal = 0.980 $Kgal$. This concept will become important later on. This is due to the fact that in this study, geopotential numbers are used first for calculating relative vertical movement of the markers from year to year. When calculating the velocity of markers (in mm/yr) from the relative geopotential numbers, the orthometric height is obtained using equation 3.4. This will be discussed further in section 3.6.

Levelling data is also frequently contaminated by systematic errors. It is therefore essential to correct these errors before the data is processed. They come from three distinct sources: atmospheric refraction, calibration of survey rods and effects of the magnetic field on certain levelling instruments.

3.2 Levelling data

The Canadian vertical network, shown in Figure 3.3, contains around 124000 km of levelling lines that have measurements dating back to 1904. It is used primarily for the realization of the Canadian Geodetic Vertical Datum (CGVD28). Between 1972 and 2000, the network was entirely re-surveyed. Since 2001 though, the GSD has performed minimal levelling for datum maintenance. This is mostly due to the use of an alternative approach using geoid modelling and the Global Navigation Satellite System (GNSS) to realize a new vertical datum used as the new Canadian vertical

control network [Véronneau et al. (2006)].

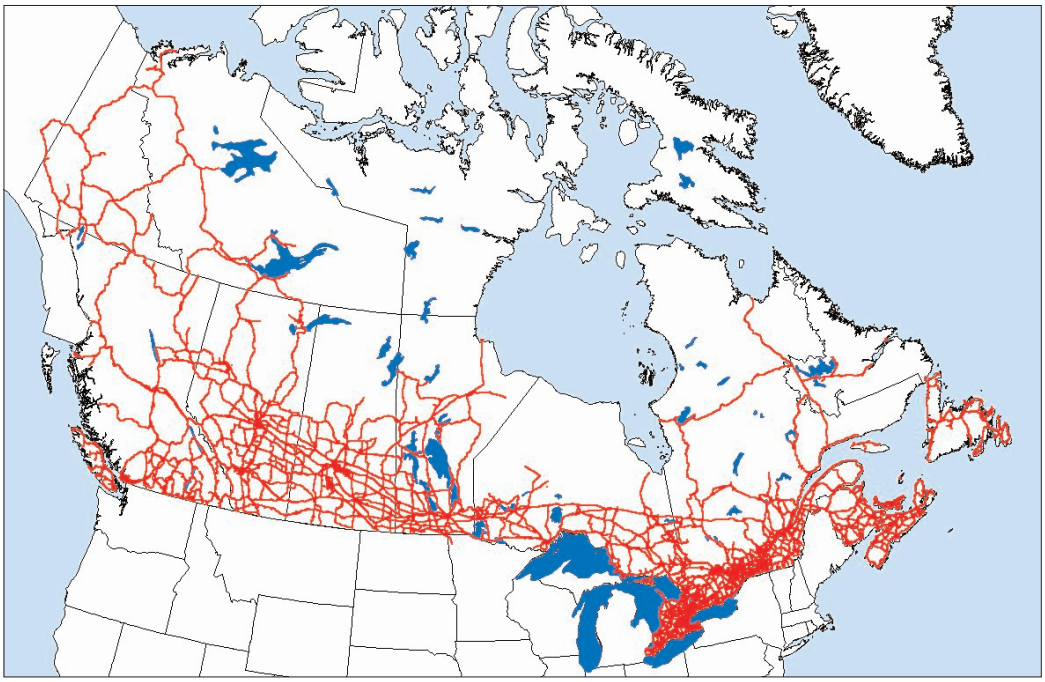

Figure 3.3: Extent of first order levelling network in Canada from Véronneau et al. (2006)

Figure 3.4 shows a close up of the levelling network for the Saint Lawrence valley. The geopotential differences published and used for this study were constructed from the results of annual survey observations dating back to 1904 in Canada. The levelling data from Figure 3.4 spans the years 1909 to 1996.

As mentioned in section 3.1, levelling data is frequently contaminated by systematic errors. The levelling data, in this case, has been corrected for atmospheric correction, calibration of survey rods and the effects of the magnetic field on the levelling instruments for which this is the case [Berube (1989)]. The data obtained had already been adjusted, and therefore the errors associated with the geopotential number differences are those resulting from the adjustment.

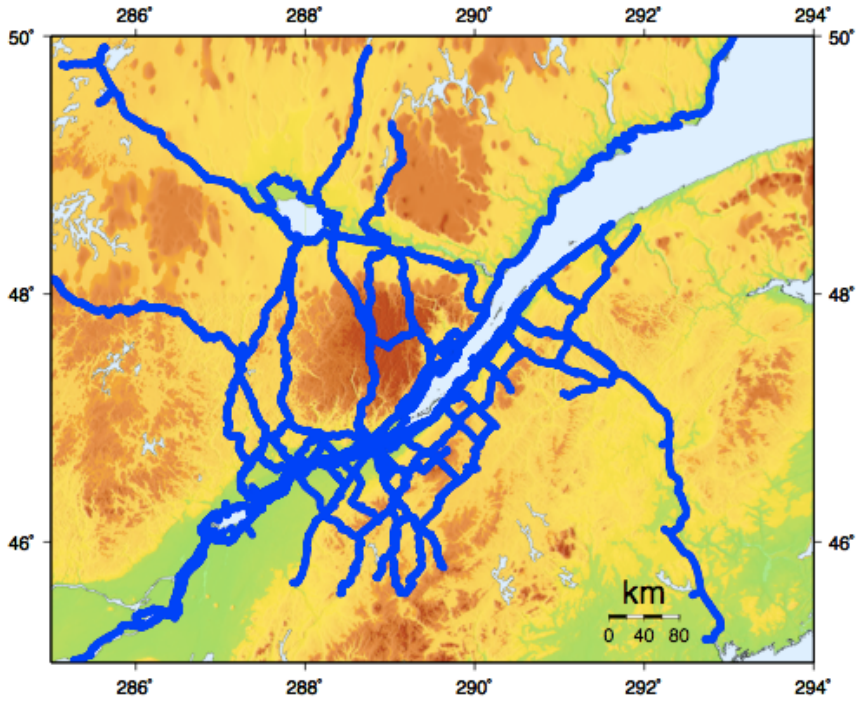

Figure 3.4: First order levelling data in the Saint Lawrence region from 1909 to 1991

3.3 Strategy for determining geopotential number differences of repeat levelling lines

The data is analyzed as a function of a temporal change in relative geopotential, meaning that altimetric markers in common from a levelling line number are compared for different epochs. Optimally, it would be best to have levelling lines that consistently have one or more markers in common, and to fix one reference point in the whole network. Unfortunately, the data was collected piecemeal. It was not until the 1970's that a conscious effort was made to remeasure lines with the purpose of detecting crustal deformation [Véronneau et al. (2006)].

For different levelling lines, new markers are added, removed, or not measured at all depending on the year. Some lines were also only partially remeasured. There are also instances where the same lines were measured starting from the opposite direction at different epochs, which had to be taken into account. As such, MATLAB subroutines were created for the sole purpose of finding matching markers from levelling lines.

Due to the large amount of geopotential number difference values involved (over 15000), only matching markers from independent levelling lines were analyzed. For levelling lines with more than two epochs in common, the relative geopotential differences of the levelling lines are presented in section 3.4.

3.4 Relative geopotential difference results of levelling lines in the CSZ

The levelling lines with multiple markers for multiple years are presented in this first section. Figure 3.5 shows the location of the levelling lines with multiple common markers for more than two epochs. It is important to note that the stars represent the starting point (relative geopotential = 0 m Kgal) for all epochs. The line number is the format used by the GSD to distinguish independent levelling lines. The levelling lines are all parallel to the Saint Lawrence river, and therefore not optimal for detecting postglacial rebound effects.

The longest levelling line with multiple markers for more than two epochs is 255. Figure 3.6 shows the difference in relative geopotential for the common markers. The levelling line starts in the Rivière-du-Loup area and follows the south side of the Saint Lawrence river until the city of Quebec with 61 markers in common. The reference year is 1955, and the markers were remeasured in 1970, 1983 and 1987.

There are two levelling lines parallel to line 255 on the north shore. The first is line 138, in which the relative geopotential differences of matching markers are presented in Figure 3.7. The line starts in La Malbaie and works its way up to Saint Simeon along the Saint Lawrence river. Overall, the line is around 30 km long and contains 13 markers. The reference year is 1962, and the markers were remeasured in 1982, 1985, 1987 and 1991.

The second levelling line parallel to line 255 on the north shore is 084. The graphical representation of the relative geopotential differences can be found in Figure 3.8. As can be seen from Figure 3.5, the levelling line starts in Baie-St-Paul and follows the

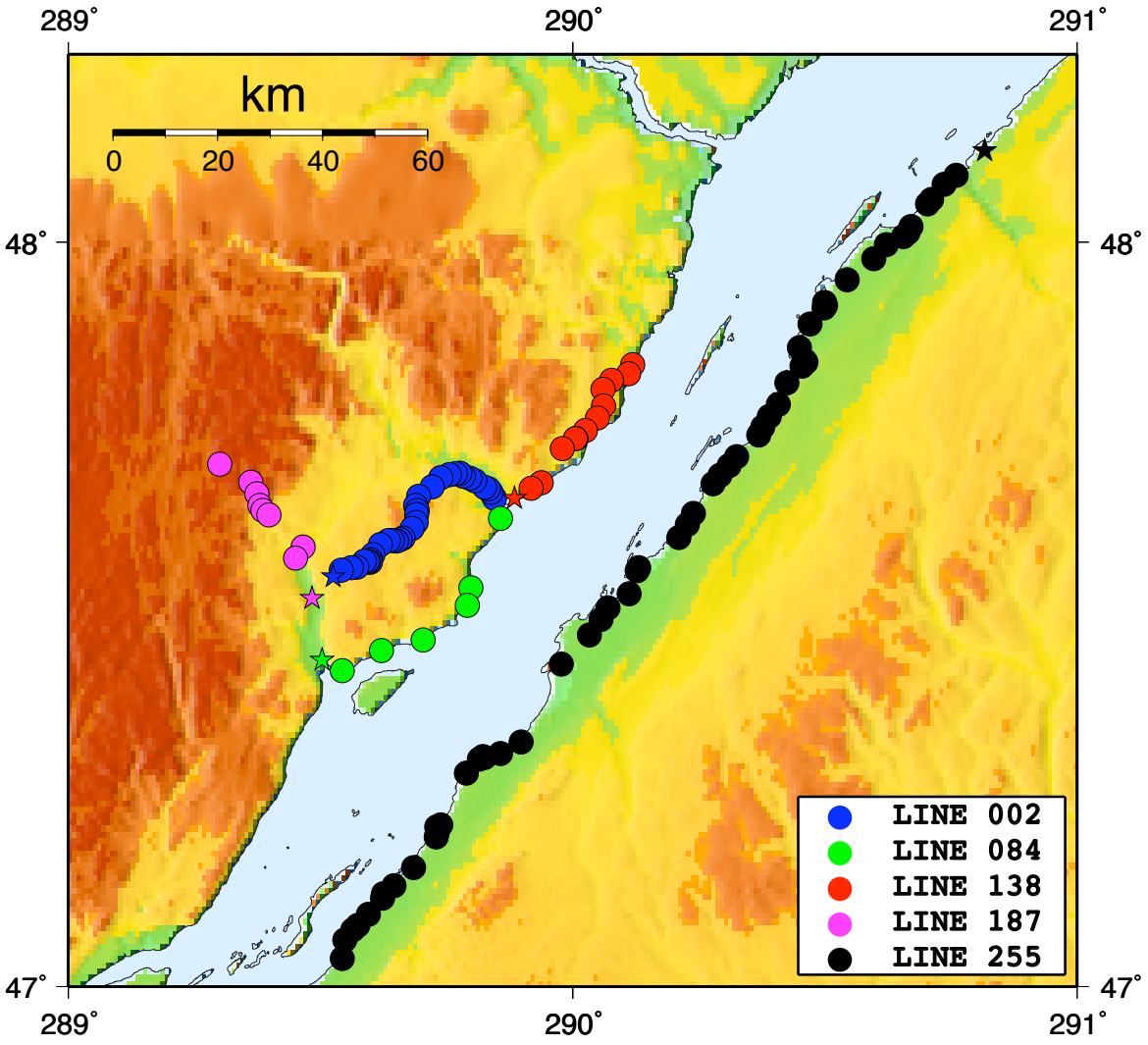

Figure 3.5: Location of levelling lines with multiple common markers in CSZ. Stars indicate reference point of levelling in graphics of relative geopotential differences

Saint Lawrence river up to La Malbaie. The levelling line contains 9 markers and spans 35 km. The reference year in this case is 1964 and the markers were remeasured in 1983 and 1991.

Other than lines 138 and 084 on the north shore, there are two levelling lines that have multiple markers for multiple years. The first is line 187 which runs perpendicular to the Saint Lawrence river on the north shore. It starts in Baie-St-Paul and spans 35 km. The relative geopotential differences of the matching markers can be seen in Figure 3.9 and contains 9 markers. Here, the reference year is 1964 and the markers

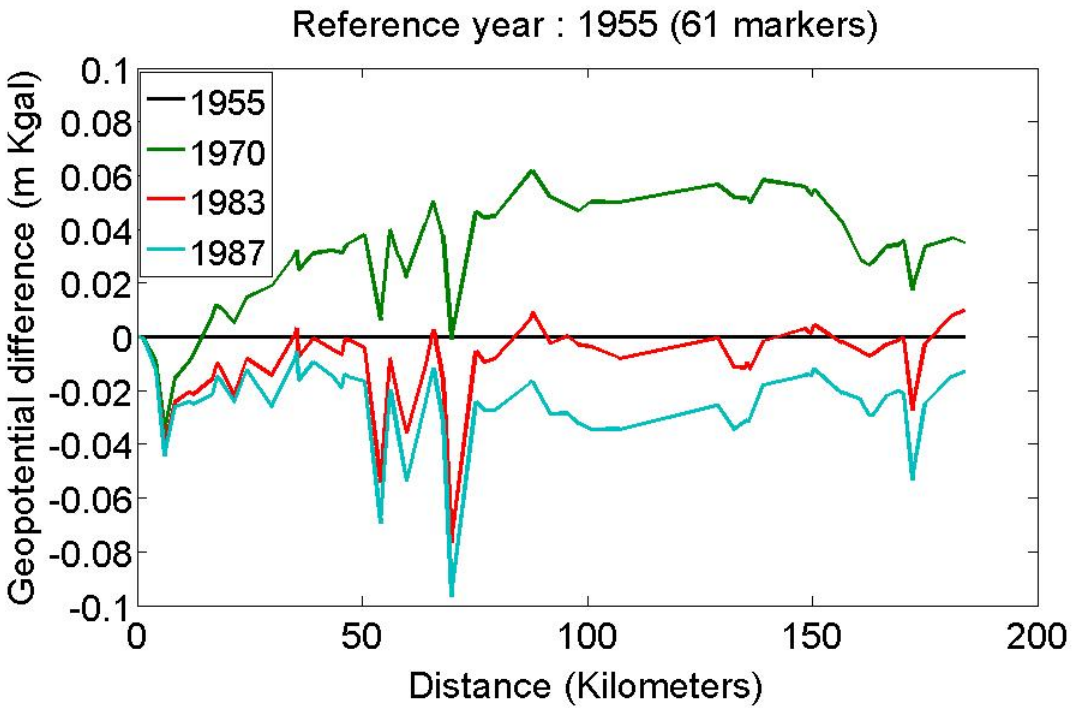

Figure 3.6: Relative geopotential difference of line 255 matching markers

were remeasured in 1983 and 1991.

Line 002 though, runs parallel to line 084 further from the shore of the Saint Lawrence river. The marker relative geopotential differences can be seen in Figure 3.10. Overall, there are 33 markers and the line is about 40 km long. The reference year for this line is 1977 and the markers were remeasured in 1985 and 1991.

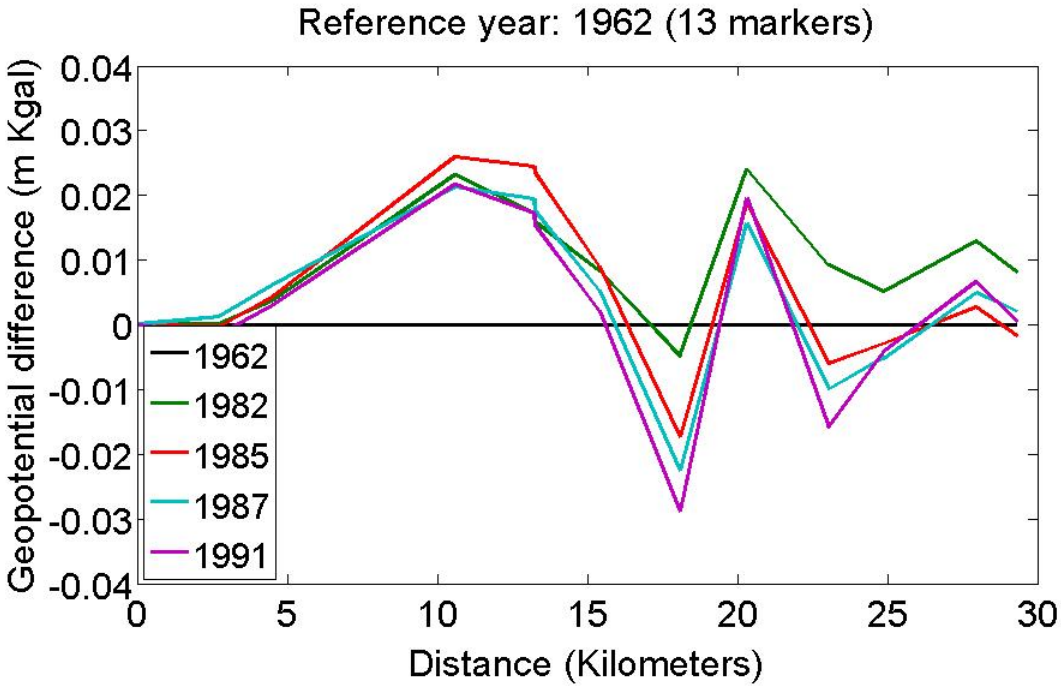

Figure 3.7: Relative geopotential difference of line 138 matching markers

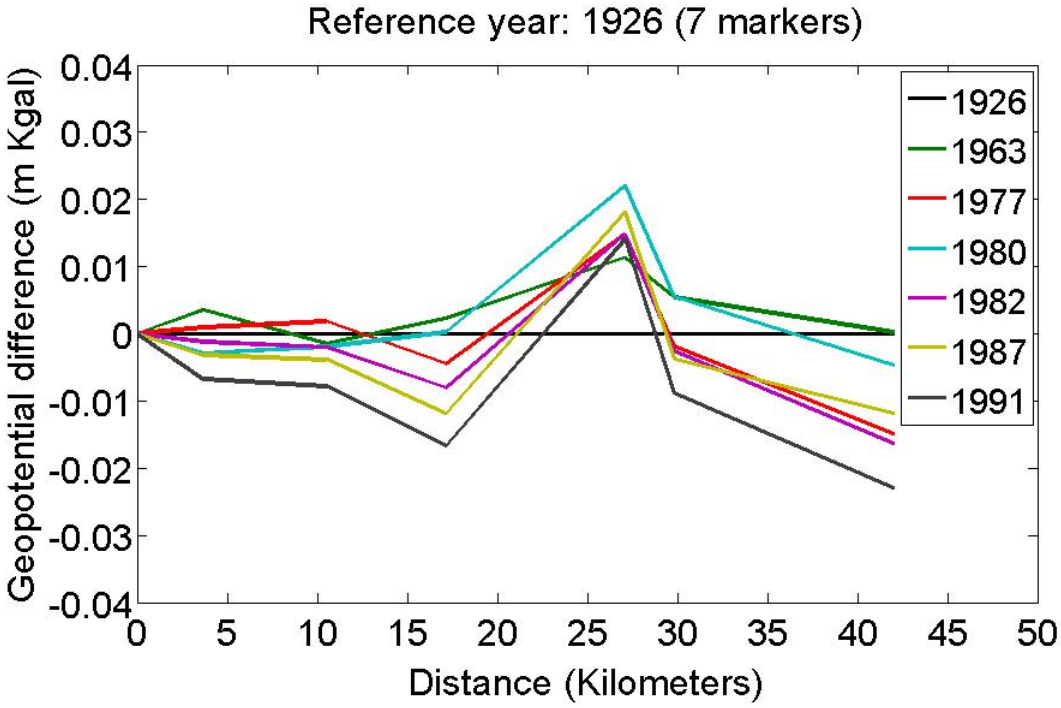

Figure 3.8: Relative geopotential difference of line 084 matching markers

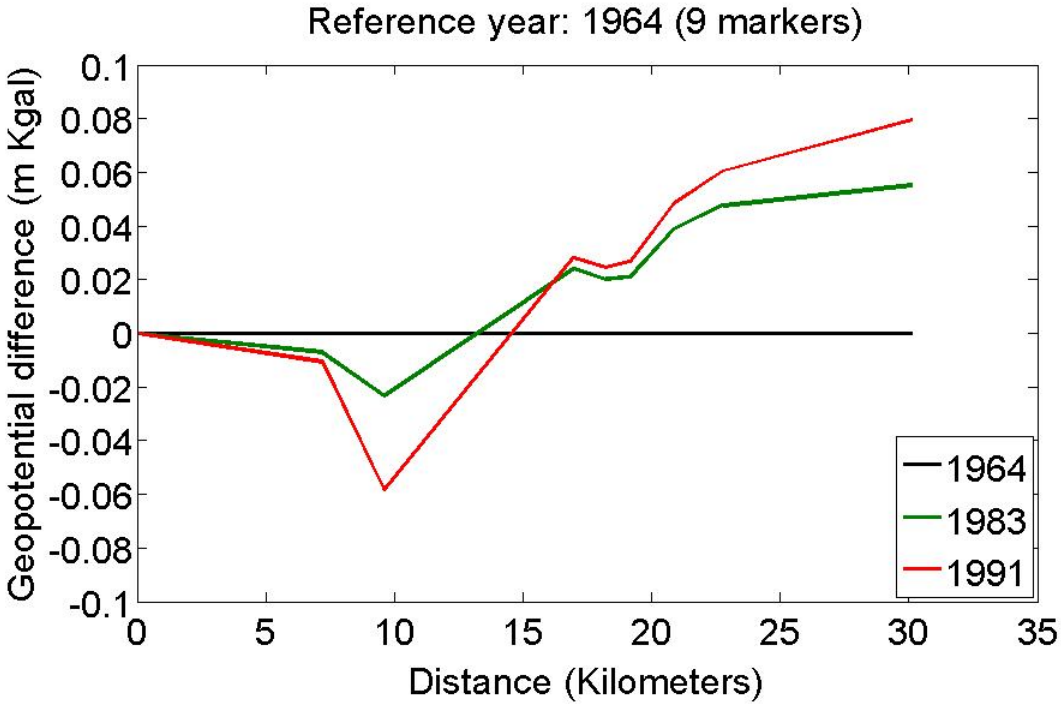

Figure 3.9: Relative geopotential difference of line 187 matching markers

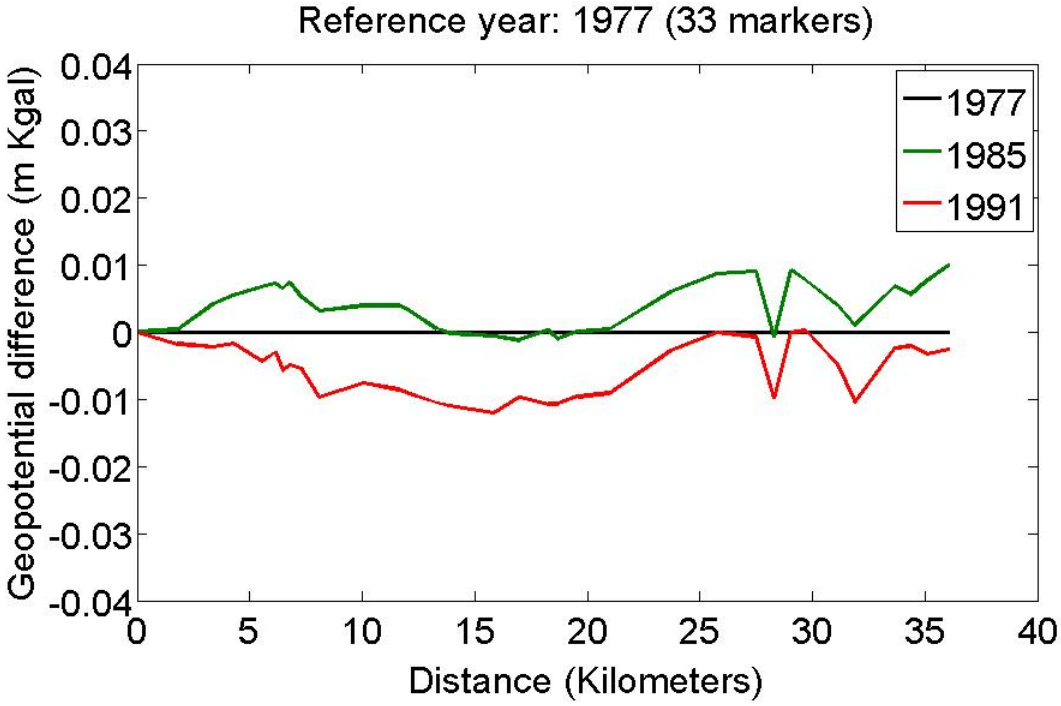

Figure 3.10: Relative geopotential difference of line 002 matching markers

The relative geopotential differences of these lines inside the CSZ show mixed results. None of the lines show a clear uplift signal between all the years. The longest line, 255, shows a complex behavior. Between 1955 and 1970, there is a clear relative uplift for all the markers in the line. But then, between 1970 and 1987, there is evidence of subsidence. The same can be observed in line 138, where between the years 1962 and 1982 an uplift signal, albeit small, is distinguishable. Between 1982 and 1991, we again see evidence of subsidence. It is even less evident for line 084, where no clear uplift signal is discernable, and neither is there evidence of relative uplift from one end of the levelling line to the other.

One reason to explain the fact that no relative uplift is evident from these levelling lines is that they run parallel to the Saint Lawrence river. As can be seen from Figure 2.4, the relative uplift follows a northwest trend, and therefore the northeast direction sees a uniform rate of uplift. Line 187 is the only levelling line that runs perpendicular to the Saint Lawrence river. As can be seen from Figure 3.9, between 1964, 1983, and 1991, the relative geopotential differences start showing relative uplift away from the Saint Lawrence river, but even here the results are mixed, as half the levelling line (closest to the Saint Lawrence river) shows indications of subsidence. The final levelling line, 002, which runs perpendicular to the Saint Lawrence river and then changes directions and follows the Saint Lawrence in a parallel direction shows subsidence as well.

The levelling lines in the CSZ zone are perpendicular to the uplift trend direction of Figure 2.4. The velocities are not derived from these lines because there is no clear vertical signal in any of these lines.

3.5 Strategy for determining the velocity of markers in levelling lines

Outside the CSZ zone, the velocity, in mm/yr, of the markers from matching levelling lines that have two epochs is derived. The velocity was calculated by taking the difference between the two geopotential numbers of the marker for the first and second year and dividing it by the number of years between the two surveys. This method is the

same for levelling lines with more than two epochs.

In order to obtain meters from m Kgal, the geopotential number difference is divided by the mean gravity value at the marker location (equation 3.4 utillizing the gal unit for the gravity value). The resulting height differences are thus orthometric height differences in meters.

In chapter 6, the velocity of the markers between the beginning and the end of the levelling line will be compared with the variation of velocity between GPS sites derived from previous GPS campaigns on CBN sites and the uplift velocities predicted by PGR models. To do this, a linear regression is fit to the levelling line values in order to determine the velocity variation. This will allow a better comparison with the GPS results.

3.6 Relative velocity results from levelling lines outside the CSZ

There are some interesting results outside the CSZ zone, including levelling lines that span to the northwest of the Saint Lawrence river where postglacial rebound becomes much more evident. These levelling lines only have two epochs compared. Figure 3.11 shows the levelling lines outside the CSZ having two epochs with common markers. Once again, it is important to note that the stars represent the starting point (relative velocity = 0 mm/yr). As explained in section 3.5, the velocity of each marker from the relative geopotential number differences are calculated for these levelling lines using the method described in section 3.5. The final relative velocities are in mm/yr.

The first of the levelling outside the CSZ zone is line 001 in Figure 3.12. The line starts about 140 km away from the Saint Lawrence river towards Rivière-du-Loup. It is located to the northeast of the CSZ on the south side of the Saint Lawrence river. Overall there are 88 markers and the reference year is 1979, with measurements taken again in 1987.

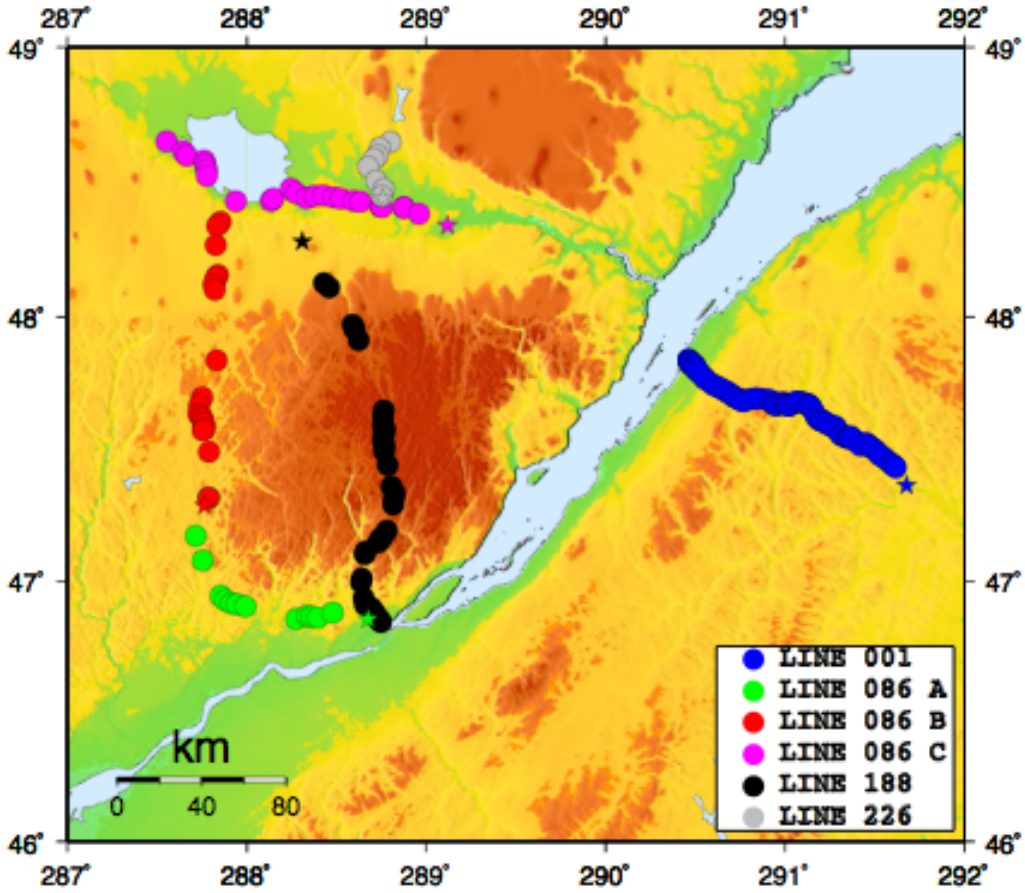

Figure 3.11: Location of levelling lines with multiple common markers outside of CSZ. Stars indicate starting point (relative velocity = 0 mm/yr) of relative velocity graphs

The other 5 levelling lines outside the CSZ are located on the north side of the Saint Lawrence river. The first of these is line 086A, where the relative velocity of the sites is shown in Figure 3.13. The line starts in Quebec City and runs parallel to the Saint Lawrence for about 140 km. There are 14 matching markers in this line and the reference year is 1919, with the levelling repeating in 1964.

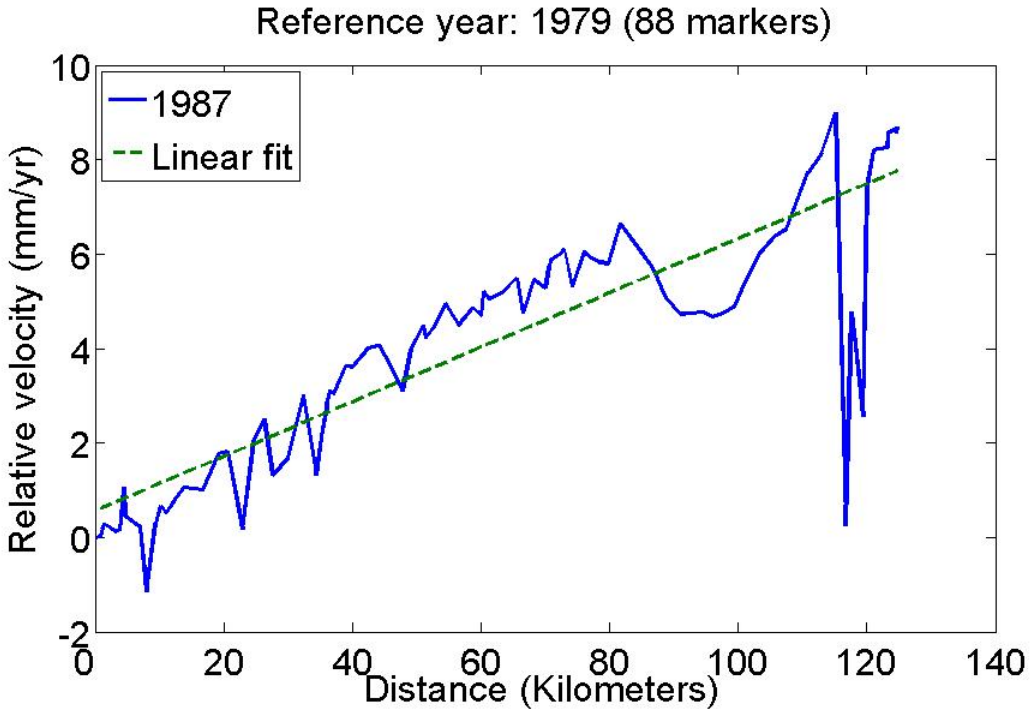

Figure 3.12: Relative velocity for markers of line 001

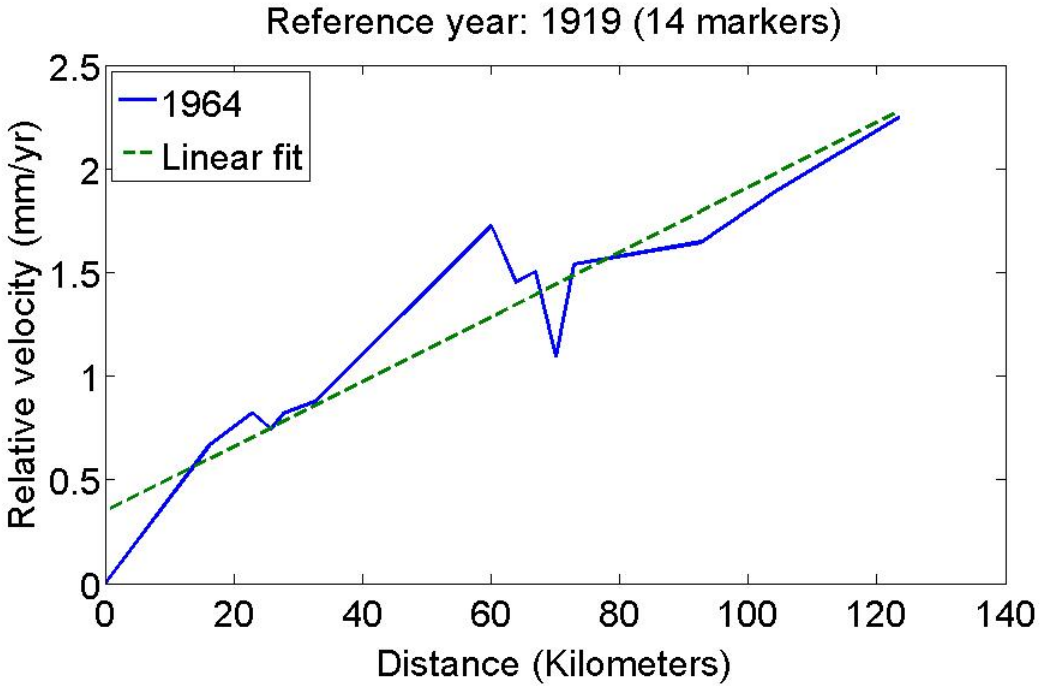

Figure 3.13: Relative velocity for markers of line 086A

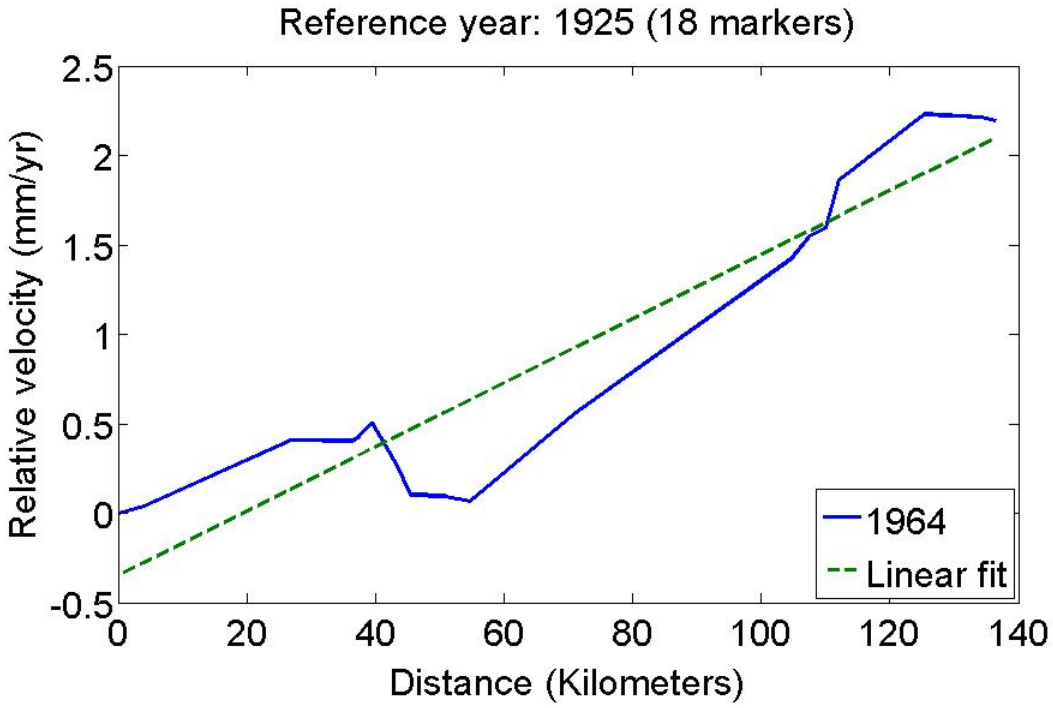

Figure 3.14: Relative velocity for markers of line 086B

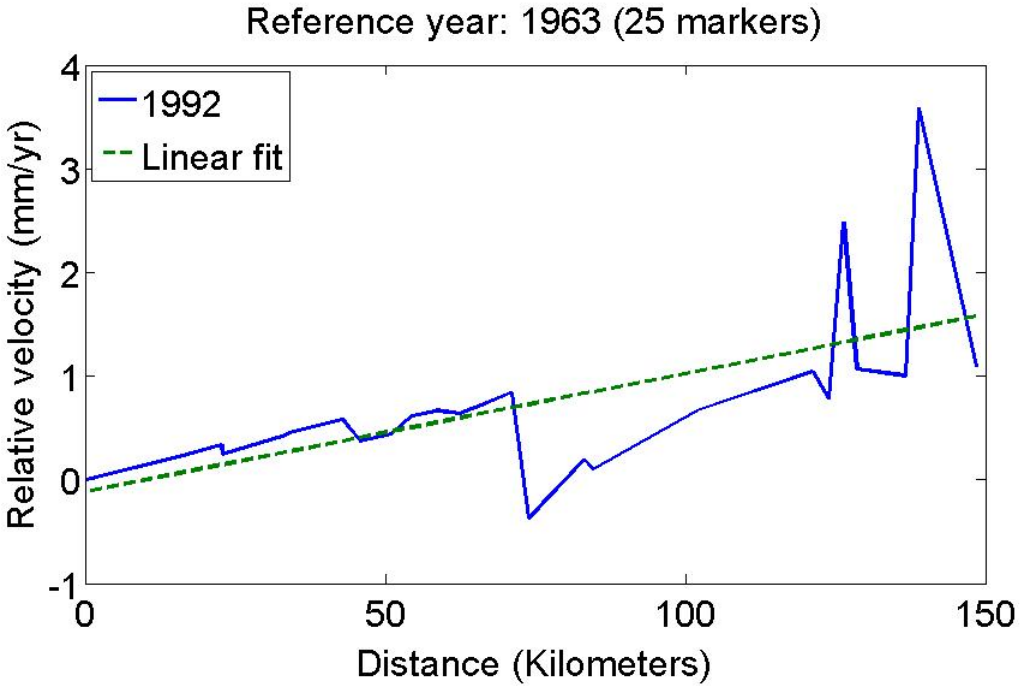

Figure 3.15: Relative velocity for markers of line 086C

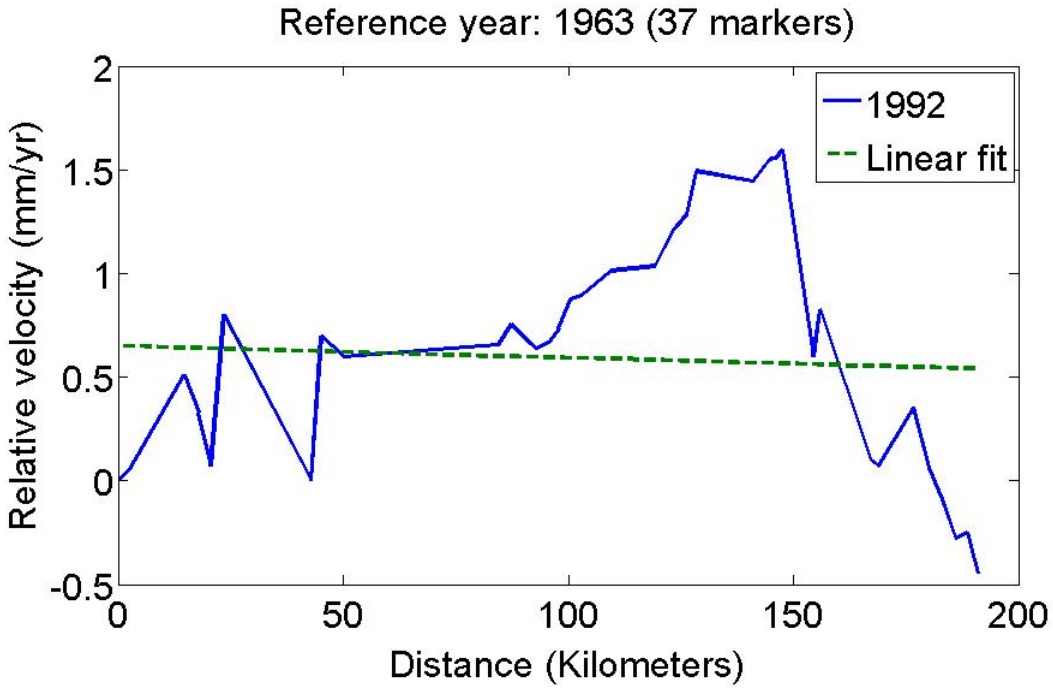

Figure 3.16: Relative velocity for markers of line 188

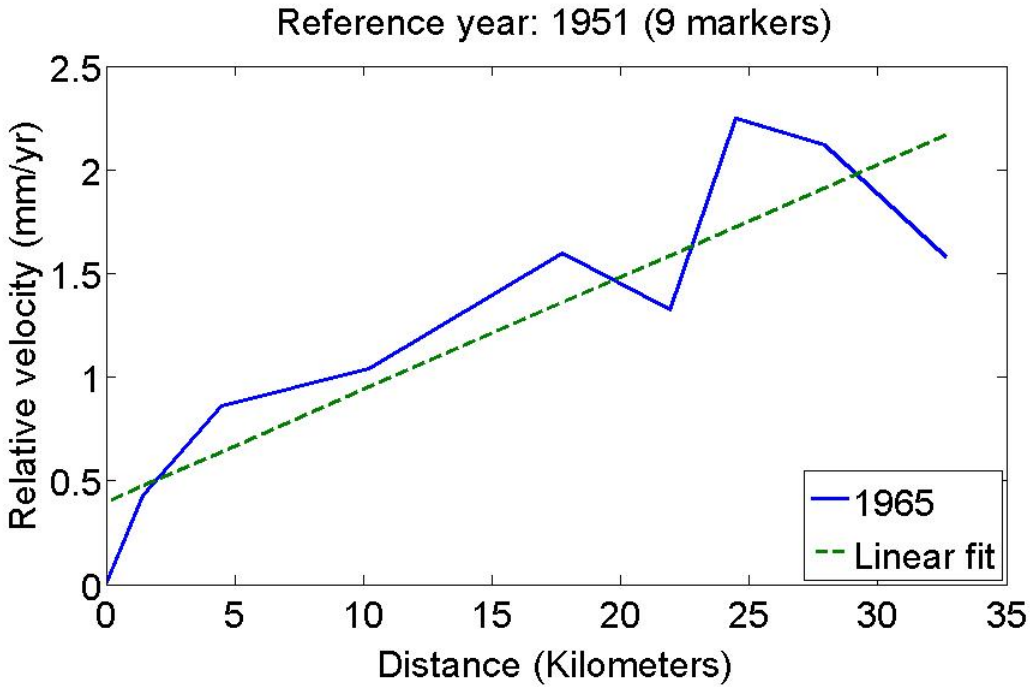

Figure 3.17: Relative velocity for markers of line 226

Levelling line 086B, in which the relative velocities are shown in Figure 3.14, runs from where line 086A ends up to Lac Saint-Jean for a length of 140 km. There are 18 markers for this levelling line, where the reference year is 1925 and the line was remeasured in 1964.

The relative velocities of the matching markers for line 086C are in Figure 3.15. The line begins east of Lac Saint-Jean and follows the lake shore westward. It is 150 km long. There are 25 matching markers between the reference year 1963 and the second levelling year of 1992.

The longest of the levelling lines with matching markers outside the CSZ is line 188, where the relative velocities of the matching markers are shown in Figure 3.16. The line is almost 200 km long and follows a straight line from Quebec City all the way to Lac Saint-Jean with 35 markers in common for reference year 1963 and the year 1992.

The final levelling line in this study outside the CSZ zone is line 226, whose relative velocity is shown in Figure 3.17. The line follows a northward path starting eastward of Lac Saint-Jean. It is 35 km long with 9 matching markers. The reference year is 1950 and the markers were remeasured in 1965.

Table 3.1 presents the linear polynomial fit equation as well as the first and last marker fit velocity and the difference between them. Here, y is the relative velocity and x is the distance.

Line	Polynomial coefficients	V_{begin} (mm/yr)	V_{end} (mm/yr)	V_{diff} (mm/yr)
001	$y = 0.058x + 0.554$	0.6	7.8	$\simeq 7$
086A	$y = 0.016x + 0.346$	0.3	2.3	$\simeq 2$
086B	$y = 0018x - 0.349$	-0.4	2.1	$\simeq 2$
086C	$y = 0.011x - 0.116$	-0.1	1.6	$\simeq 2$
188	$y = -0.001x + 0.650$	0.7	0.5	$\simeq 0$
266	$y = 0.054x + 0.396$	0.4	2.2	$\simeq 2$

Table 3.1: Results of velocity fit of levelling lines outside CSZ.

The pattern of relative uplift is increasing in a perpendicular direction to the Saint

Lawrence river going northwest. This is most evident in line 001 on the south shore, and lines 086A, 086B, and 226 on the north shore. For line 001, the variation from the beginning of the levelling line to the end of the levelling line is around 7 mm/yr. For lines 086A and 086B, the variation is 2 mm/yr for both lines going northwest. For line 226, the variation is also 2 mm/yr. Less evident are lines 086C, 188 on the north shore. For line 086C, the variation from the beginning of the levelling line to the end is around 2 mm/yr, and for line 188, the variation is around 0 mm/yr.

In chapter 6, the variation of the velocities of these levelling lines outside the CSZ will be compared with the variation of velocity between GPS sites derived from previous GPS campaigns on CBN sites and the uplift velocities predicted by PGR models. The PGR model predicted velocities are at the same locations as the GPS velocities from previous GPS campaigns.

Chapter 4

GPS data collection and processing

This chapter is divided into 3 sections. The first section will give a description of the conventional processing method with the use of academic GPS processing software (BERNESE v5.0) for monitoring crustal deformation. The ITRF2000 and IGS reference stations to tie local networks to a global reference frame will also be discussed. The second section will present the 2005 GPS campaign. It will be described first because it is the conventional GPS processing method for high precision crustal deformation monitoring. This will include an overview of the data collection strategy, the data used for the processing, the processing strategy, ambiguity resolution results and the coordinate results. The third section will thus, in turn, detail the 1991 GPS campaign and the significant differences between it and the 2005 campaign due to pre IGS era observations. It will be concluded with the ambiguity resolution results and final coordinate results for the 1991 campaign.

4.1 Conventional processing for high precision GPS networks

The BERNESE v5.0 software developed at the University of Berne is used for the data processing. It is used by two of the seven IGS analysis centers to contribute to

the maintenance of the ITRF and the calculation of IGS products, including precise satellite ephemerides and clocks. It has also been utilized significantly in processing millimeter accuracy networks for monitoring crustal deformation in Canada [Mazzotti et al. (2003), Mazzotti et al. (2005)].

Figure 4.1 shows a flowchart of the processing strategy.

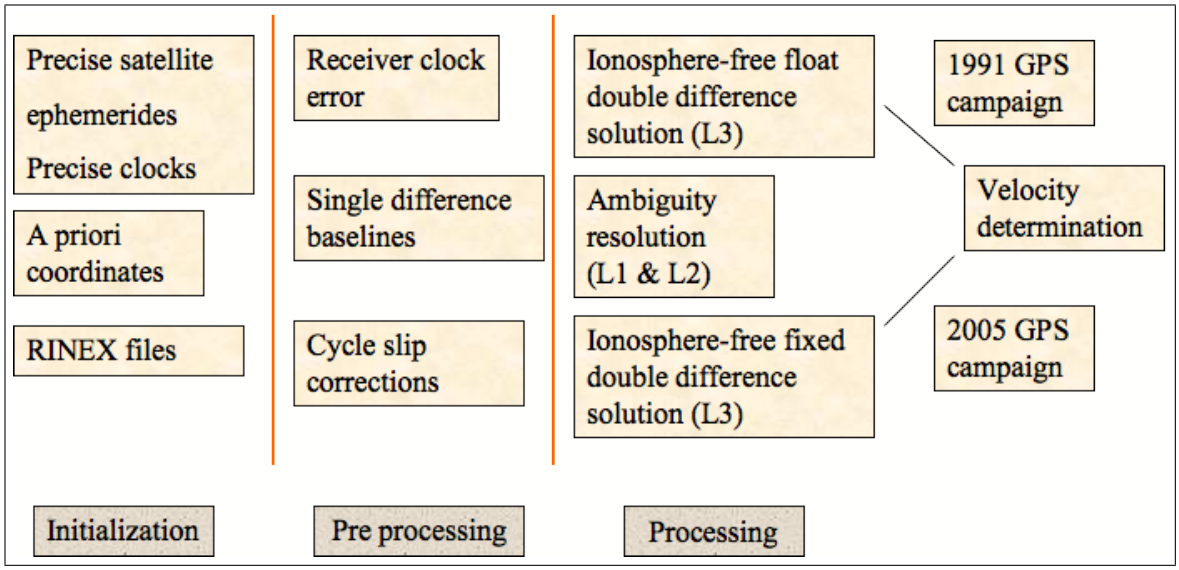

Figure 4.1: Processing strategy of high precision GPS networks using BERNESE v5.0

The processing strategy can be divided into three separate blocks. The three blocks are termed initialization, pre processing, and processing.

Initialization

The first subsection of the initialization stage is error reduction and modelling through the use of several important parameters.

1. **Precise ephemerides and clocks:** These are provided by the International GNSS Service (IGS). The files contain satellite position and clock information where the satellite positions are stored in an Earth-fixed system for a table of epochs of fifteen minute intervals and the satellite clocks for five minute intervals

with a precision of less than 5 cm and 0.1 ns, respectively. The satellite positions and clocks are computed using a network of known ground stations distributed globally. The tracked orbits are computed at seven analysis centers using a variety of independent GPS softwares such as BERNESE, GIPSY[1], and GAMIT [Herring et al. (2006)]. The solutions are combined by the IGS into weighted final orbits. IGS final orbits and clocks are usually available two weeks after the last observation.

2. **Antenna PCV:** These are defined as the difference between the electrical phase center from the geometric phase center of the antenna where the former is defined as the location at which the satellite signal is captured and the latter is taken as a geometrical reference point. The latter can be the Antenna Reference Point (ARP), as defined by IGS[2] and is needed in order to connect the GPS measurements to the monument or point whose position has to be determined. The offsets are obtained from the IGS in the ANTenna information EXchange (ANTEX) format.

3. **Global Ionosphere models:** As will be explained later on in section 4.1, the quasi-ionospheric free (QIF) strategy is applied for the ambiguity resolution. Global ionosphere models greatly increases the percentage of ambiguities resolved. Global Ionosphere Maps (GIM) are generated on a daily basis at CODE, one of the IGS analysis centers located at the University of Berne, using data from about two hundred GPS sites of the IGS. The final IONosphere map EXchange (IONEX) files are available three days after the observation day. More information can be obtained at the University of Berne website[3].

4. **Ocean loading and solid earth tides**: Two types of station corrections also have to be taken into account which arise from the same phenomenon. The Earth is affected by tidal forces from other celestial bodies, most notably from the Moon and the Sun. This causes periodical motions known as ocean loading and solid earth tides. Ocean loading is the crustal deformation caused by the changing mass distribution due to ocean tides. It is a site specific phenomenon and the parameters necessary for the computation of its effect can be obtained from the

[1] http://gipsy.jpl.nasa.gov/orms/goa/index.html
[2] ftp://igscb.jpl.nasa.gov/igscb/station/general/igs_01.pcv
[3] http://www.cx.unibe.ch/aiub/ionosphere.html

free ocean tide loading provider website[4]. In the Charlevoix region, this effect can achieve a vertical motion of up to 2 cm. Solid earth tides are the equivalent of ocean tides but on land and are modelled according to the IERS Conventions 2003 [McCarthy and Petit (2004)] in BERNESE. For baselines shorter than 100 km, this effect can be safely neglected as it cancels out during the double differencing. For longer baselines, such as those including IGS stations, this effect must be taken into account because the effect can achieve upwards of 30 cm in the radial and 5 cm in the horizontal directions [Kouba and Héroux (2001)].

The second subsection of the initialization block is the calculation of a priori coordinates and velocities. As a few centimeters accuracy is required for the approximate coordinates of the stations in order to neglect errors introduced by linearization and to improve ambiguity resolution, the a priori coordinates for the campaign sites need to be calculated. A widely used method to achieve this accuracy is to use precise point positioning (PPP) with IGS precise orbits and clocks. PPP is a GPS processing method in which the station coordinates are calculated using zero difference phase and code observations, or in other words, using only one receiver. The BERNESE software has the capability of doing PPP processing with enough accuracy (< 5 cm) for the resulting coordinates to be implemented as a priori coordinates of the unknown sites. BERNESE also has a module that calculates a priori velocity vectors from the NUVEL-1A plate tectonic model [Demets et al. (1994)] that will be used as a priori velocities for the final velocity determination. More information can be found in chapter 20 of Hugentobler et al. (2004).

The third subsection of the initialization block is the validation of the information in the field log and with that in the RINEX observation file headers. This includes checking that the antenna height from the marker is the same in the observation file than the field log, the antenna and receiver types are identical, and that the marker names are correct.

[4]httpp://www.oso.chalmers.se/∼loading

Pre processing

The second block of the processing strategy is the pre processing. The three subsections are calculating the clock error of the receivers, creating the single difference baselines, and checking and correcting the cycle slips.

The receiver clock errors are estimated at this point to simplify the pre processing, specifically the screening for cycle slip detection and correction. It is possible to compute the receiver clock errors with sufficient accuracy (< 1 μs) using zero difference code measurements. The procedure requires satellite clock corrections which can be obtained from broadcast navigation messages or from precise IGS orbits files or IGS clock files.

The second subsection in the pre processing block is the creation of the single difference baselines. There are three automatic strategies:

1. OBS-MAX: The baselines are created by taking into account the number of common observations for the associated stations. From all possible combinations, a set of baselines with maximum common observations is chosen.
2. SHORTEST: The baseline length is used as the criterion to create the set of shortest baselines. This is useful if you want to create the same set of baselines for each session.
3. STAR: In this strategy, the baselines are built by selecting one reference station and connecting it with all remaining stations. If the reference station is not chosen manually, the reference station will be selected automatically in a way that the sum of the length of all baselines is minimized.

The third pre processing step is the detection and correction of cycle slips. This occurs when a loss of lock between the receiver and satellite causes a jump in the instantaneous accumulated phase by an integer number of cycles. Cycle slips can have several causes which include obstruction of the satellite signal due to trees, buildings or other large objects, low signal-to-noise ratio due to rapidly changing ionospheric conditions, multipath, or low satellite elevation angle. In BERNESE, the cycle slip

detection program is called MAUPRP, which utilizes single difference observation files to form and analyze different linear combinations of phase observations. The program checks all observations and finds time intervals which are corrupted by cycle slips. If possible, it repairs the cycle slip, otherwise it marks the observation period as an outlier or a new unknown ambiguity parameter must be introduced [Hugentobler et al. (2004)].

Processing

The third block is the processing itself. It comprises three steps: calculating first a ionosphere-free (L3) float ambiguity solution, resolving the ambiguities on L1 and L2, and calculating a ionosphere-free ambiguity fixed solution by introducing the integer values obtained in the previous step.

The first processing step, the ionosphere-free float solution with unresolved integer ambiguities allows the estimation of more accurate a priori coordinates, if necessary, as well as allowing the estimation of troposphere parameters which will be used as known parameters in the ambiguity resolution.

The second processing step is the ambiguity resolution. For small GPS networks, the recommended ambiguity resolution method for medium (10-100 km) to long (100-2000 km) baseline lengths and long observation sessions is QIF. In principle, an initial least squares adjustment using both L1 and L2 frequencies give real-valued ambiguity estimates with which a corresponding ionosphere-free bias is computed. The difference between this real-valued bias and the integer L3 bias obtained using the real integer ambiguity values acts as the selection of the best pair of integers. Figure 4.2 shows the graphical representation of this process.

A more detailed description of the algorithm can be found in chapter 8 of Hugentobler et al. (2004). Due to the length of the baselines, and because the processing is occurring on both the L1 and L2 frequencies separately, the ionospheric refraction causes a bias in the determination of the ambiguity resolution. To reduce this ionospheric bias, we use the GIM deterministic model described in section 4.1.

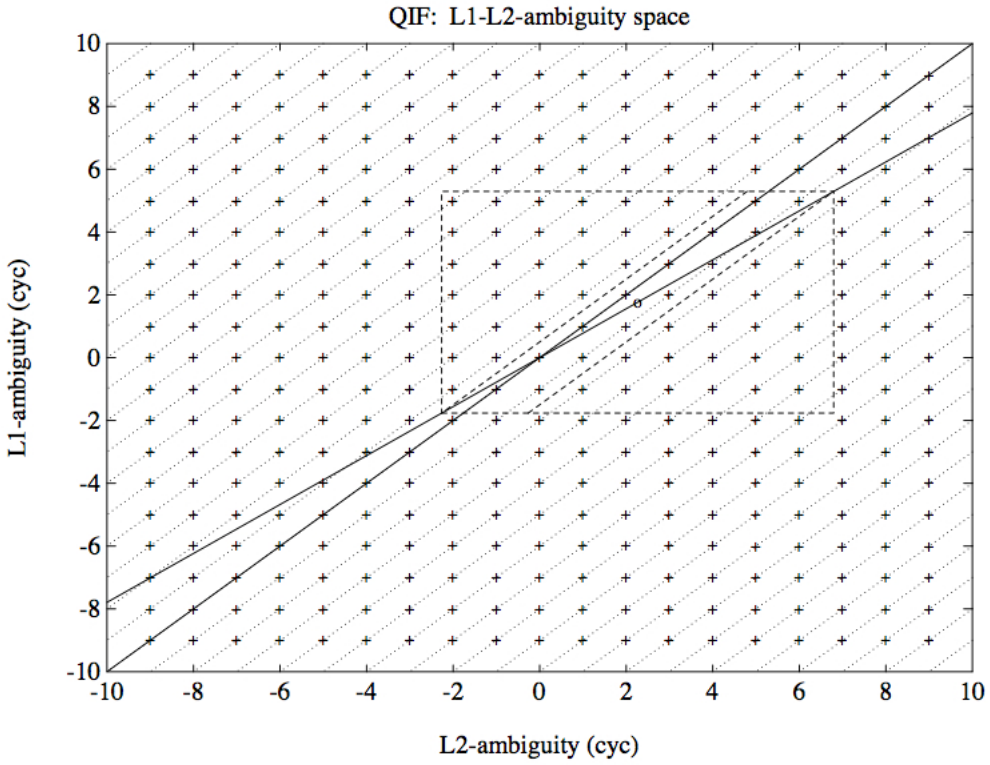

Figure 4.2: Graphic representation of QIF ambiguity resolution strategy from Hugentobler et al. (2004)

The third and final processing step to obtain site coordinates is the calculation of the final ionosphere-free ambiguity fixed solution. We estimate troposphere parameters using Dry Niell Mapping [Niell (1996)]. In this final step, we also constrain the IGS reference stations by fixing their nominal position and velocities with a certain a priori standard deviation (in this case, 1 mm and 1 mm/yr, respectively) to tie the local network to ITRF2000.

4.1.1 ITRF2000

Positions in space or on Earth are neither observables nor absolute quantities and therefore have to be determined with respect to some reference frame. In the past, each technique used its own Terrestrial Reference Frame (TRF) which meant that a multitude of TRF coexisted, each with systematic biases that made them difficult to

compare. This fact led the International Union of Geodesy and Geophysics (IUGG) and the International Association of Geodesy (IAG) to adopt a unique TRS, called the International Terrestrial Reference System (ITRS) [McCarthy and Petit (2004)] for Earth science applications.

The realization of the ITRS, termed the International Terrestrial Reference Frame (ITRF), is obtained from various analysis centers that combine the results of station positions and velocities collected using space and earth based geodetic techniques such as Very Long Baseline Interferometry (VLBI), Lunar and Satellite Laser Ranging (LLR and SLR), GPS, and Doppler Orbitography Radiopositioning Integrated by Satellite (DORIS). At the time of the data processing, ITRF2000 [Altamimi et al. (2002)] was the latest realization and as such was used for tying the Charlevoix network to the ITRS.

The common strategy in crustal deformation monitoring with GPS is thus to choose IGS sites surrounding the entire network in which the nominal positions and velocities are known at a significant enough level (i.e. a millimeter) to constrain them to their positions and velocities at the mm and mm/yr level [McCarthy and Petit (2004)].

4.2 2005 GPS campaign

4.2.1 Overview

The 2005 GPS data was collected as a collaboration between the Pacific Geoscience Center (PGC) and the CRG at Université Laval from the 20^{th} to the 27^{th} of July. These are days 201 through 208 of the year. Consecutive 48 hour sessions were measured using dual frequency ASHTECH UZ-12 receivers and ASH701945C_M choke ring antennas with a sampling rate of 30 seconds. Overall, 16 stations were surveyed, including the reoccupation of 7 sites which have been observed in 1991 and new stations installed for future reoccupation. Only the 7 reoccupied stations were processed in this study because the site velocities can only be derived for reoccupied sites. Figure 4.3 shows the location of the 2005 campaign sites, Figure 4.4 shows the sites processed in both 2005

and 1991, and Table 4.1 shows the session characteristics of the processed stations.

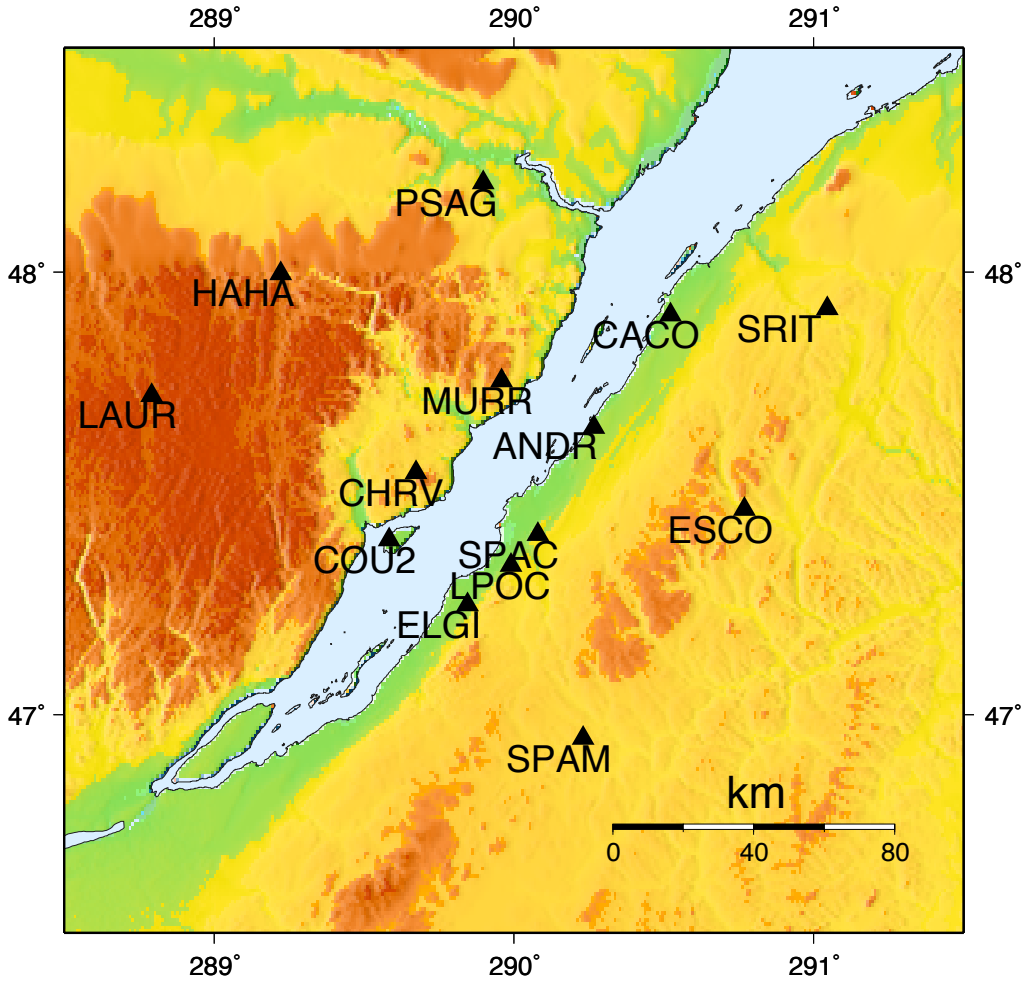

Figure 4.3: 2005 GPS network

The session characteristics of the sites and sessions not used are in Appendix A (Table A.1). Other site characteristics, such as approximate longitude and latitude of the sites can be found in Table A.3 of Appendix A.

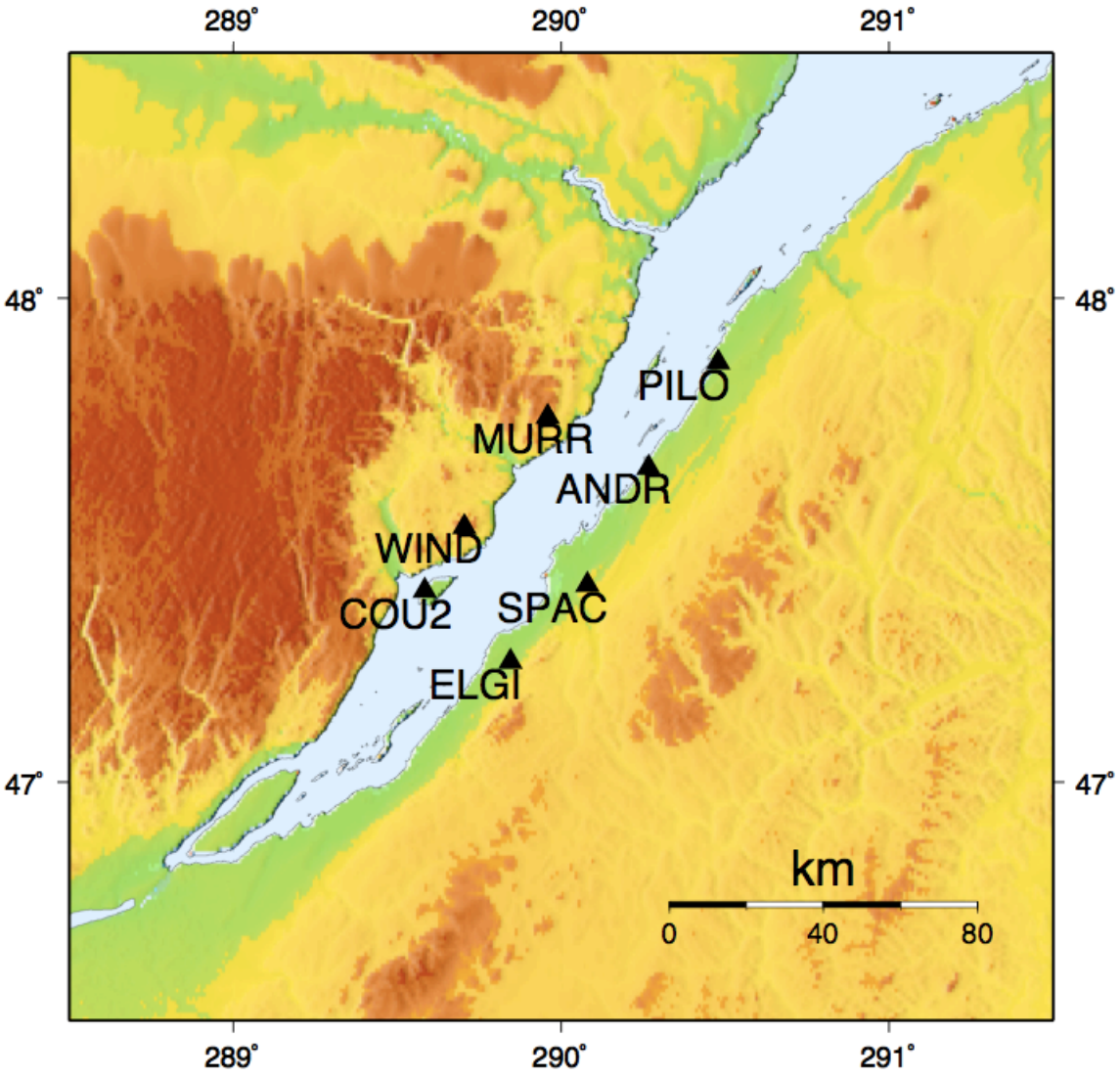

Figure 4.4: 2005 GPS network sites used for processing with the 1991 GPS campaign sites

Station name	DOY	Observation period (UTC)		
		Start	End	Length (hrs)
ANDR	202	00:00:00	23:59:30	24
	203	00:00:00	23:03:30	23.07
COU2	205	00:00:00	23:59:30	24
	206	00:00:00	23:34:00	23.57
ELGI	205	00:00:00	23:59:30	24
	206	00:00:00	23:59:30	24
MURR	202	00:00:00	23:59:30	24
	203	00:00:00	23:59:30	24
PILO	202	00:00:00	23:59:30	24
	203	00:00:00	23:59:30	24
SPAC	202	00:00:00	23:59:30	24
	203	00:00:00	23:59:30	24
WIND	205	00:00:00	23:59:30	24
	206	00:00:00	23:59:30	24
	207	00:00:00	23:59:30	24
	208	00:00:00	23:59:30	24

Table 4.1: 2005 GPS data characteristics of sessions processed

4.2.2 Processing strategy

Table 4.2 shows a summary of the important parameters and processing specifics of the 2005 GPS campaign.

Parameter	Description
Processing interval	Daily
Number of sites	7
IGS reference stations	5
Sampling rate	30 seconds
A priori coordinates of sites	PPP-BERNESE
Satellite ephemerides	Precise IGS
Satellite clocks	Precise IGS
Antenna phase centers	ANTEX IGS
Elevation cut-off angle for processing	3°
Single difference baseline creation	STAR Strategy
Ocean loading model	GOT00.2
A priori ionosphere model	GIM-CODE
Ambiguity resolution	QIF
Troposphere parameter estimation	Dry Niell 24 per day

Table 4.2: 2005 processing strategy description

The sessions are processed at 24 hour intervals for the 7 sites in figure 4.3. The a priori coordinates are calculated using the PPP processing engine in BERNESE that employs precise satellite orbits and clocks and the zero difference phase and code observations. The PPP processing engine also determines a priori site velocities according to the NUVEL-1A model as described in section 4.1. The satellite orbits and clocks used, as well as the antenna phase center variations, are those from the IGS. The single difference baselines were created using the STAR strategy as described in section 4.1. A permanent GPS station, named LPOC that can be seen in figure 4.3 was used as

the reference station for all the sessions. This site was chosen because it was the only station collecting data during the entire campaign (other than the IGS sites). As for the ionosphere model and ocean loading parameters, deterministic GIM's were obtained from the IGS processing at CODE and the loading parameters were obtained from the ocean loading site described in section 4.1 using the GOT00.2 ocean model [Ray (1999)].

Figure 4.5 shows the location of the IGS sites used in the 2005 campaign and Table 4.3 describes the characteristics of the IGS sites. The official ITRF2000 coordinates were constrained to an a priori standard deviation of 1 mm in the processing.

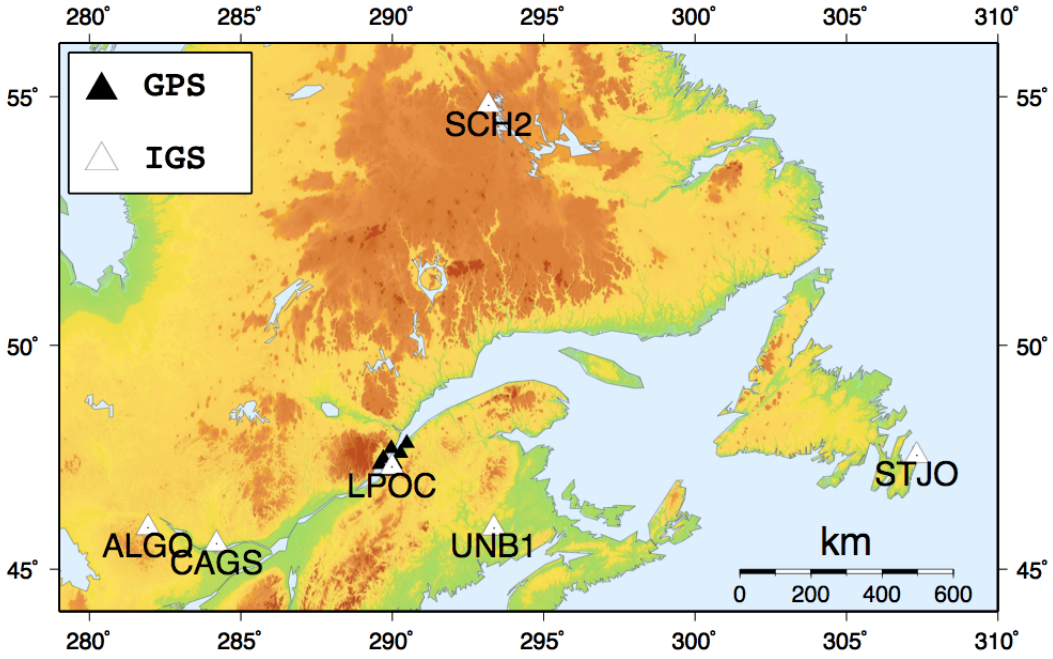

Figure 4.5: Location of IGS GPS sites for 2005 GPS campaign

SITE	Receiver	Antenna	λ, °E	ϕ, °N	h (m)
ALGO	AOA BM ACT	AOAD/M_T	-78.071	45.959	202.00
CAGS	ASHTECH Z-XII3	ASH700936A_M	-75.807	45.585	235.00
LPOC	ASHTECH Z-XII3	ASH701945E_M	-70.009	47.341	103.24
SCH2	AOA SNR-12 ACT	AOAD/M_T	-66.833	54.832	498.18
STJO	AOA BM ACT	AOAD/M_T	-52.678	47.595	152.84
UNB1	TPS LEGACY	JPSREGANT_DD_E	-66.642	45.950	22.83

Table 4.3: Specifications of IGS stations used in processing

Ambiguity resolution

The ambiguity resolution method used is QIF, which is a baseline by baseline method. Table 4.4 shows a summary of the 2005 ambiguity resolution results in percentage where $\hat{\sigma}_o$ is the a posteriori sigma of unit weight (normalized to one-way L1 phase observable at zenith). Table A.4 in Appendix A shows a more detailed ambiguity resolution success rate for each day. It is also to be noted that if the L1 ambiguity is resolved, so is the L2 ambiguity. This applies to all the QIF ambiguity resolution results presented in this work.

DOY	Number of baselines	Average baseline length (km)	Average of ambiguities resolved (%)	Average of $\hat{\sigma}_o$(mm)
202	9	417	77	1.4
203	9	417	79	1.3
204	5	717	84	1.2
205	8	458	87	1.1
206	8	458	84	1.3
207	6	603	80	1.4
208	6	603	76	1.5

Table 4.4: Summary of 2005 campaign ambiguity resolution using QIF strategy

4.2.3 Final coordinates of 2005 campaign

The final coordinates are obtained from using the ambiguity resolution results from section 4.2.2 and keeping the IGS sites constrained to 1 mm of their nominal ITRF2000 positions. The troposphere was modeled using Dry Niell Mapping with 24 zenith delay parameters estimated per day and 4 gradient parameter estimates per 24-hour session. Table 4.5 are the results that are used to determine the velocity vectors in chapter 5.

SITE	λ, E (dms)	ϕ, N (dms)	h (m)	σ_E (mm)	σ_N (mm)	σ_h (mm)
ANDR	-69 43 57.58071	47 39 06.85587	163.209	3.4	3.3	4.4
COU2	-70 24 51.50363	47 23 57.60402	62.982	3.4	3.3	4.5
ELGI	-70 09 14.83221	47 15 02.81065	99.643	3.4	3.3	4.3
MURR	-70 02 29.82304	47 45 23.42165	652.541	3.4	3.3	4.8
PILO	-69 31 14.25291	47 52 08.40899	56.882	3.4	3.3	4.4
SPAC	-69 55 09.00548	47 24 35.82803	229.667	3.4	3.3	4.3
WIND	-70 17 44.26804	47 31 47.08201	740.444	3.3	3.3	4.1

Table 4.5: 2005 GPS campaign coordinate results with a 1σ confidence interval in local geodetic

4.3 1991 GPS campaign

4.3.1 Overview

The 1991 GPS data was collected over a five day period by the GSD. It was collected between the 20^{th} and the 23^{rd} of September, and then on September 27^{th}. These are days 263-266 and 270 of the year. Overall, 11 stations were observed along both sides of the Saint Lawrence river for 4-5 hours on 2 to 3 separate days. Since the GPS satellite constellation was still incomplete in 1991, sufficient sky coverage was only available for a certain period of the day, which explains the short session lengths. Figure 4.6 shows a map of the stations.

The sampling frequency was at 10 seconds using ASHTECH P-XII3 receivers and dual frequency ASH700228B antennas. Figure 4.6 shows the sites observed in 1991, and Figure 4.4 shows the sites processed in this research. Table 4.6 shows the important observation sessions characteristics for the 7 sites used in the processing. One of these sites, COUD, could not be remeasured in 2005 due to the decreased visibility of the sky caused by the growth of trees around the site. As such, a new marker was installed about 150 meters away in an area characterized by a clear horizon and named COU2. A terrestrial tie was made between the two sites in November 2005. It is described

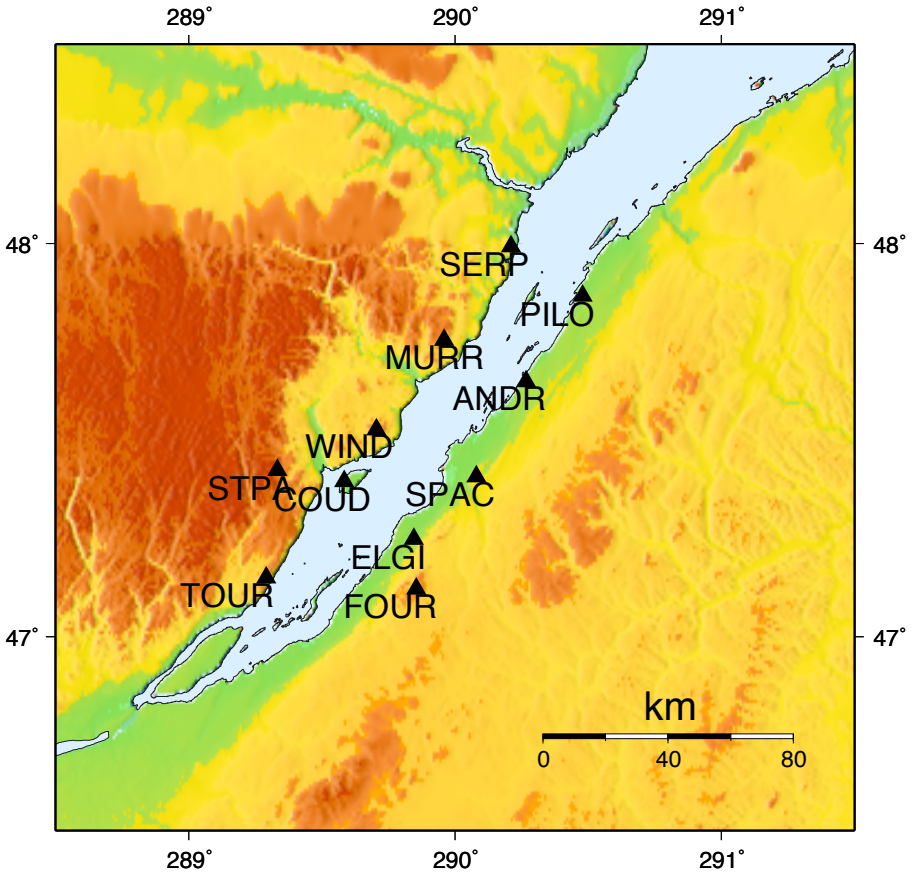

Figure 4.6: 1991 GPS network

in appendix B. The other 4 were not processed as they were not remeasured in 2005 due to inaccessibility. This accessibility is caused by growth of trees around the site or the sites have been destroyed. Session characteristics for these 4 other stations can be found in Appendix A (Table A.2). Other site information, including longitude and latitude, can also be found in Appendix A (Table A.3).

Station name	DOY	Observation period (UTC)		
		Start	End	Duration (hrs)
ANDR	263	13:49:40	19:29:50	5.67
	264	13:24:10	19:32:50	6.14
COUD	265	13:46:10	19:41:10	5.92
	266	13:44:10	19:10:20	5.44
ELGI	265	13:48:10	19:16:20	5.47
	266	13:42:40	19:10:50	5.47
MURR	263	13:55:10	18:11:10	4.27
	264	13:46:40	19:21:40	5.58
	265	13:43:10	19:15:40	5.54
PILO	263	13:53:10	19:25:20	5.54
	264	13:44:40	19:23:40	5.65
SPAC	264	13:54:40	19:20:20	5.43
	265	13:50:10	19:17:10	5.45
	270	13:34:40	19:00:20	5.43
WIND	263	13:59:10	19:25:10	5.43
	265	13:44:10	19:17:50	5.56
	270	13:32:10	19:01:10	5.48

Table 4.6: 1991 GPS data characteristics of sessions processed. Figure 4.4 shows the location of the sites processed

4.3.2 Processing strategy

Compared to 2005, the 1991 data set is characterized by the following major differences:

- The data quantity is significantly reduced. The average session length, as can be seen in Table 4.6, is between 5 and 6 hours per session with a total of 2-3 sessions per site. Since this is the case, the network adjustment was done with all the observations at once, and not on a daily basis.
- The IGS did not exist yet, and as such there are no IGS precise orbits. Fortunately, precise orbits from the Scripps Orbit and Permanent Array Center (SOPAC) are

available. The orbits were recalculated in 2001 by SOPAC with respect to the ITRF2000 reference frame with an accuracy of < 5 cm.

- The SOPAC orbits do not include precise clocks. As such, broadcast information was used as an alternative. Since a differential approach is used, the clocks are only necessary in order to obtain the transmission time of the satellites. They are also used to calculate the receiver clock error (section 4.1). Their quality is not critical.

- The number of known reference stations is significantly reduced. The only reference station is ALGO, 600 km away, with a sampling rate of 2 minutes. The specifications of the station can be found in Table 4.3 where, at the time, the receiver was a ROGUE SNR-8 and the antenna was a AOAD/M_B.

- No ionosphere model (GIM) is available for 1991. This means that the ambiguity resolution using the QIF strategy is less successful. A different approach, described below, is therefore used to calculate the ambiguities.

Table 4.7 shows an at-a-glance description of the important parameters and processing specifics of the 1991 GPS campaign.

For the above mentioned reasons, a slightly different strategy for analyzing the data was adopted. A first minor problem, due to the unavailability of precise satellite clocks in 1991, is that it is not possible to obtain accurate enough a priori coordinates for the campaign sites using the PPP processing engine from BERNESE. In order to solve this issue, the 2005 final coordinates are extrapolated backwards in time to 1991 using the a priori NUVEL-1A velocities instead. These turned out to be sufficient for the cycle slip screening process, and ultimately the ambiguity resolution. If not, iterating with a ionosphere-free float solution as the new a priori coordinates would also be a possibility.

Special care and attention was paid to baseline definition in order to have better ambiguity resolution. As mentioned above, only one reference station was in close proximity to the network (ALGO), 600 km away, and it had a low sampling rate (2 minutes). Also, no other stations were observing throughout the entire campaign. Therefore, the STAR strategy is not applicable for baseline definition.

Parameter	Description
Processing interval	Total
Number of sites	7
Sampling rate of campaign sites	10 seconds
IGS reference stations	1
Sampling rate of reference station	2 minutes
A priori coordinates of sites	NUVEL-1A
Satellite ephemerides	Precise SOPAC
Satellite clocks	Broadcast SOPAC
Antenna phase centers	ANTEX IGS
Elevation cut-off angle for processing	3°
Single difference baseline creation	OBS-MAX Strategy
Ocean loading model	GOT00.2
A priori ionosphere model	None
Ambiguity resolution (inner network) to reference station	L5/L3 QIF
Troposphere parameter estimation	Dry Niell 1 (5 h)

Table 4.7: 1991 Processing strategy description

Instead, the OBS-MAX strategy (section 4.1) is used instead. The internal geometry of the Charlevoix network is resolved and fixed first using the widelane/narrowlane ambiguity resolution strategy before tying it, as a whole, to the reference station ALGO. The widelane/narrowlane strategy, also called widelaning [Hugentobler et al. (2004)], is divided into two steps. First, the L5 (or widelane) ambiguities are resolved for the baselines formed (using OBS-MAX) with the sites from the Charlevoix network. In a subsequent run, the L3, or ionosphere-free, linear combination is processed introducing the integer widelane ambiguities and solving for the narrow lane ambiguities. This leads to the final ambiguity fixed solution. Table 4.8 shows the baselines formed and ambiguity resolution success for the inner network. $\hat{\sigma}_o$, the a posteriori sigma of unit weight (one-way L1 phase observable at zenith), is 3.1 mm.

DOY	Baseline	Length(km)	Ambiguities resolved	% resolved
263	ANDR-MURR	26	16/16	100
	ANDR-PILO	29	26/30	87
	ANDR-WIND	45	30/36	83
264	ANDR-PILO	29	32/34	94
	MURR-PILO	41	30/38	79
	PILO-SPAC	59	34/36	94
265	COUD-ELGI	26	26/30	87
	COUD-MURR	49	32/36	89
	COUD-WIND	17	30/34	88
	SPAC-WIND	31	32/36	89
266	COUD-ELGI	26	26/30	87
270	SPAC-WIND	31	40/46	87

Table 4.8: 1991 inner Charlevoix network ambiguity resolution using widelaning

Next, each station, on each day, is formed as a baseline with ALGO and the ambiguity resolution strategy QIF is run with the fixed station coordinates of the Charlevoix sites obtained using the widelaning strategy. For each day, the baseline with the highest success rate of ambiguity resolution was kept for the final adjustment. Table 4.9 shows the baselines formed, and in bold, the baseline kept for the final adjustment with the internal network baselines from Table 4.8.

The final adjustment involves now keeping the ALGO site constrained to its nominal ITRF2000 position and doing the final adjustment with the Charlevoix site coordinates left to float. The baselines used are those from Table 4.8 and the ones in bold from Table 4.9 with resolved ambiguities.

Table 4.10 shows the coordinates of ALGO after the ambiguity resolution of the baselines in bold of Table 4.9. This can be used to judge the quality of the solution after the ambiguity resolution. The difference between the a priori and the new corrected value shows that the a priori values of the campaign sites were fairly accurate to better than 1 cm.

DOY	Baseline	Length(km)	Ambiguities resolved	% resolved	$\hat{\sigma}_o$(mm)
263	**ALGO-ANDR**	**663**	**16/18**	**89**	**1.5**
	ALGO-MURR	644	4/14	29	1.2
	ALGO-PILO	685	14/18	78	1.6
	ALGO-WIND	619	18/24	75	1.4
264	ALGO-ANDR	663	14/22	64	1.7
	ALGO-MURR	644	0/20	0	1.5
	ALGO-PILO	685	0/20	0	1.5
	ALGO-SPAC	**644**	**20/26**	**77**	**1.3**
265	**ALGO-ELGI**	**623**	**16/20**	**80**	**1.7**
	ALGO-MURR	644	12/22	55	1.7
	ALGO-SPAC	644	12/22	55	1.8
	ALGO-WIND	619	12/18	67	1.7
266	ALGO-ELGI	623	6/20	30	1.9
270	**ALGO-SPAC**	**644**	**16/26**	**62**	**1.5**
	ALGO-WIND	619	8/22	36	1.7

Table 4.9: Results of QIF ambiguity resolution for baselines with ALGO station. Bold lines are baselines kept for the final adjustment

DOY	Parameter	IGS a priori value	New value	Correction (mm)	$\hat{\sigma}_o$ (mm)
263	h (m)	200.946	200.935	-11.0	1.9
	ϕ, N (dms)	45 57 20.87952	45 57 20.87988	11.1	1.1
	λ, E (dms)	-78 04 16.91429	-78 04 16.91396	7.2	0.9
264	h (m)	200.957	200.948	-8.9	2.3
	ϕ, N (dms)	45 57 20.87959	45 57 20.87980	6.5	1.1
	λ, E (dms)	-78 04 16.91432	-78 04 16.91430	0.4	0.8
265	h (m)	200.945	200.938	-7.7	2.3
	ϕ, N (dms)	45 57 20.87959	45 57 20.87984	7.7	1.2
	λ, E (dms)	-78 04 16.91454	-78 04 16.91401	11.5	1.3
270	h (m)	200.931	200.936	5.2	2.4
	ϕ, N (dms)	45 57 20.87976	45 57 20.87978	0.6	1.1
	λ, E (dms)	-78 04 16.91409	-78 04 16.91389	4.3	0.8

Table 4.10: Coordinates of ALGO after ambiguity resolution for highlighted baselines in Table 4.9

4.3.3 Final coordinates of 1991 campaign

Table 4.11 shows the coordinate solutions of the 1991 campaign in which the four ALGO baselines chosen in table 4.9 are combined with the inner Charlevoix resolved ambiguity baseline. The ALGO site is held constrained to 1 mm of its nominal 1991 position and the Charlevoix sites are left to float. One troposphere delay parameter is estimated for each day using Dry Niell Mapping functions. In 2005, 24 delays were estimated per day, but due to the short session lengths, only one delay is estimated.

SITE	λ, E (dms)	ϕ, N (dms)	h (m)	σ_E (mm)	σ_N (mm)	σ_h (mm)
ANDR	-69 43 57.56988	47 39 06.85368	163.156	3.4	3.3	5.0
COU2	-70 24 51.49295	47 23 57.60194	62.933	3.5	3.4	5.7
ELGI	-70 09 14.82184	47 15 02.80848	99.606	3.5	3.4	5.9
MURR	-70 02 29.81237	47 45 23.41957	652.491	3.4	3.3	4.9
PILO	-69 31 14.24231	47 52 08.40674	56.836	3.4	3.3	5.0
SPAC	-69 55 08.99516	47 24 35.82597	229.615	3.4	3.3	4.7
WIND	-70 17 44.25772	47 31 47.07989	740.389	3.4	3.3	4.8

Table 4.11: 1991 GPS campaign coordinate results with a confidence interval of 1σ in local geodetic

In chapter 5, the coordinate results from Table 4.5 and Table 4.11 are used to calculate the velocity vectors of the 7 CSZ sites in both the horizontal and vertical component, which is the last step in Figure 4.1.

Chapter 5

CSZ deformation from GPS

This chapter is divided into two sections. The first section will discuss the method in which the velocities are calculated from GPS coordinates of the 1991 and 2005 campaigns. The second section will present both the horizontal and vertical velocity vectors resulting from this calculation. There is also a subsection on calculating the velocities of the CSZ sites for the purpose of mapping the horizontal results onto the stable North America (NOAM) Plate.

5.1 Velocity determination

In order to obtain the site velocities, station velocities are setup as unknown constant parameters in the least squares adjustment position solution in BERNESE. The module that does this is called ADDNEQ2. A priori velocities are obtained from the NUVEL-1A tectonic plate model, as described in section 4.1. The nominal velocities of the IGS reference frame stations are treated as known parameters and are constrained to these values. For the local CSZ network, only one reference station, ALGO, was installed and running in both 1991 and 2005 in close proximity (600 km away) from the network. Both the nominal ITRF2000 position and velocity vector of the ALGO site are constrained to 1 mm and 1 mm/yr respectively.

5.2 Velocity results

The following section contains the velocity results in both the horizontal and vertical components of the coordinate results presented in Tables 4.5 and 4.11. Presented first will be the horizontal velocities in ITRF2000. Then, the calculation of the North America ITRF2000 rotation pole velocities of the sites will be discussed and the results will be presented. The horizontal velocities mapped into the stable NOAM will thus be subsequently presented. Finally, the vertical velocities of the stations will be presented. As mentioned previously, the nominal position and velocity vector of the ALGO site are held constrained at 1 mm and 1 mm/yr, respectively.

5.2.1 Horizontal velocities in ITRF2000

Figure 5.1 shows the horizontal velocities of the Charlevoix network sites with respect to the ITRF2000 frame. In table 5.1, the values of the horizontal velocities in the local geodetic frame are presented where the correlation is that between the north and east velocity components.

SITE	V_E (mm/yr)	V_N (mm/yr)	σ_E (mm/yr)	σ_N (mm/yr)	correlation
ANDR	-16.5	5.0	0.32	0.30	0.11
COU2	-16.3	4.7	0.31	0.31	0.05
ELGI	-15.9	4.9	0.32	0.30	0.04
MURR	-16.2	4.7	0.31	0.30	0.12
PILO	-16.0	5.1	0.32	0.30	0.14
SPAC	-15.7	4.7	0.31	0.29	0.09
WIND	-15.7	4.8	0.30	0.29	0.09

Table 5.1: Horizontal velocities of stations in ITRF2000 with a 1σ confidence interval

The velocities vary between -16.5 mm/yr and -15.7 mm/yr in the eastern component, where the negative values indicate a westward drift. The north component varies between 4.7 and 5.1 mm/yr. For both the east and north component, the standard deviation hovers around 0.3 mm/yr at the 1σ confidence interval. Combined, the two

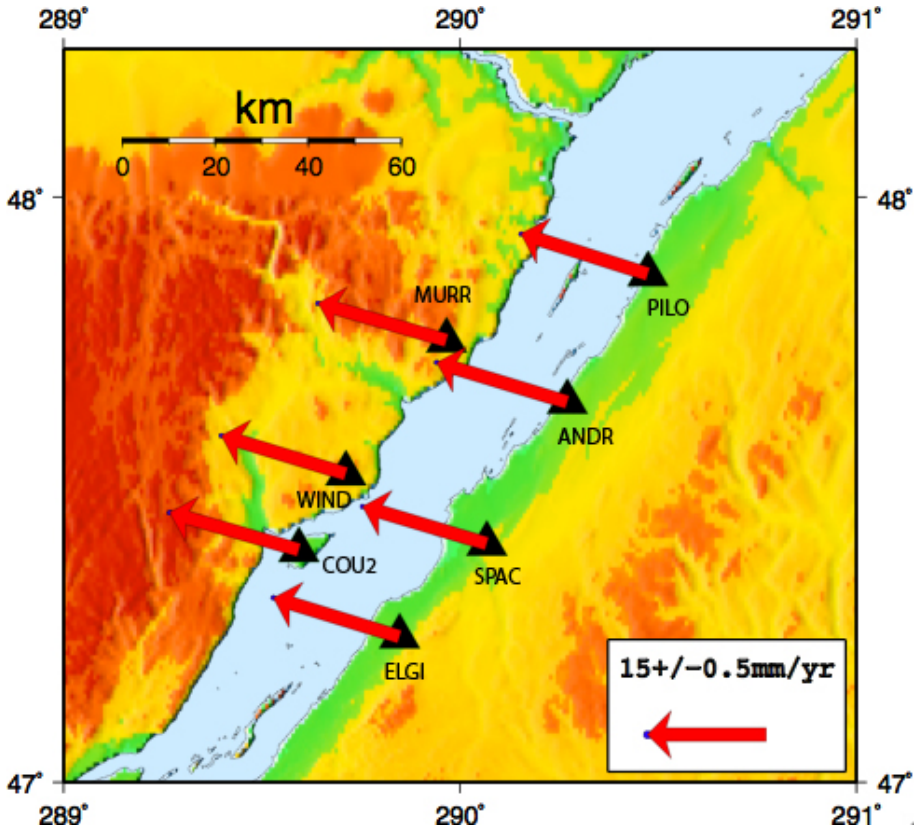

Figure 5.1: Horizontal velocities of stations in ITRF2000

components give a horizontal velocity of about 16.8 mm/yr. These results are comparable to the North American Plate predicted velocities of eastern Quebec in ITRF2000 from Henton et al. (2006).

5.2.2 Calculating horizontal site velocities of Charlevoix sites on North American Plate

The horizontal velocities calculated in section 5.2.1 obtained are in the ITRF2000 frame which means the velocities include the motion of the rigid NOAM Plate. The interest lies in the relative velocities of these sites with respect to the stable NOAM Plate. In order to obtain these results, it is necessary to subtract the site velocities of a rigid plate. This is done by subtracting a rotation vector of NOAM to the campaign sites. The rotation vector applied is that of Altamimi et al. (2002), the values of which are

given a little later in this section. It is important to note that the NOAM rotation pole does not account for vertical motion, meaning that the rigid plate only moves horizontally. The representation of the rigid movement of a plate on a sphere can be modelled by a rotation vector given by its pole and its angular velocity. On a sphere, such a movement does not induce strain. Figure 5.2 shows a uni-dimensional graphical representation of the geometrical situation, where d is the distance from the pole. The method can be extended to the two and three dimensional case.

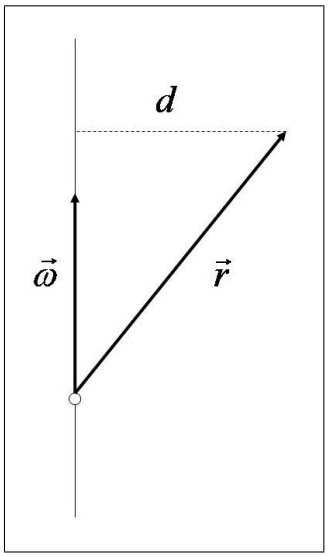

Figure 5.2: Uni-dimensional representation of rotating body velocity determination from Kreyszig (1979)

The velocity vector $\vec{v}$ can be represented in the form:

$$\vec{v} = \vec{\omega} \times \vec{r} \tag{5.1}$$

$\vec{\omega}$: angular velocity vector of rotation pole

$\vec{r}$: position vector of site

$\vec{\omega}$ can be decomposed as:

$$\vec{\omega} = \omega \cdot \vec{n} \tag{5.2}$$

$\vec{n}$: unit direction vector of axis of rotation

ω : angular speed of rotation pole

where:

$$\vec{n} = \begin{pmatrix} \cos\phi_{NA} \cdot \cos\lambda_{NA} \\ \cos\phi_{NA} \cdot \sin\lambda_{NA} \\ \sin\phi_{NA} \end{pmatrix} \tag{5.3}$$

The parameter values of the NOAM absolute rotation pole [Altamimi et al. (2002)] are:

ϕ_{NA}: -5.036 °N

λ_{NA}: -83.144 °E

ω : 0.194 °/M.y.

where ω is in degree/millions of years.

5.2.3 Results of horizontal site velocities on North American Plate from ITRF2000

Table 5.2 shows the velocity vectors in the local geodetic frame of the Charlevoix sites. These intermediate velocities are used later for the mapping of the ITRF2000 velocities

of section 5.2.1 in the stable North America frame. MATLAB subroutines were coded in order to calculate these values and subtract them from the ITRF2000 velocities as such a module does not exist in BERNESE v5.0.

SITE	V_E (mm/yr)	V_N (mm/yr)
ANDR	-16.7	5.0
COU2	-16.7	4.7
ELGI	-16.6	4.8
MURR	-16.7	4.9
PILO	-16.7	5.1
SPAC	-16.6	4.9
WIND	-16.7	4.8

Table 5.2: Velocities of Charlevoix sites from ITRF2000 North America rotation pole

5.2.4 Horizontal velocities on the stable North American Plate

Figure 5.3 shows the relative horizontal velocities on stable North America after the subtraction of the North America rotation pole velocities of Table 5.2 from the horizontal ITRF2000 velocities of Table 5.1. Table 5.3 shows the values of these site velocities as well as the standard deviation at the 1σ confidence interval. Here, the correlation is between the north and east components.

The velocities vary between 0.17 mm/yr and 0.98 mm/yr in the eastern component and varies between 0.02 mm/yr and -0.21 mm/yr in the north component, where the negative values indicate a southward drift. For both the east and north component, the standard deviation hovers around 0.3 mm/yr at the 1σ confidence interval. Combined, the two components give a horizontal velocity that is no greater than 1 mm/yr.

By installing permanent GPS stations in the CSZ, the standard deviation of the coordinates would be reduced and would give a better velocity resolution as well as allowing the modelling of GPS noise for better error estimates. The variation in the short term velocities could be detected. Also, because of the increase in time resolution due to continuous GPS stations, seasonal signals and potential offsets caused by seismic

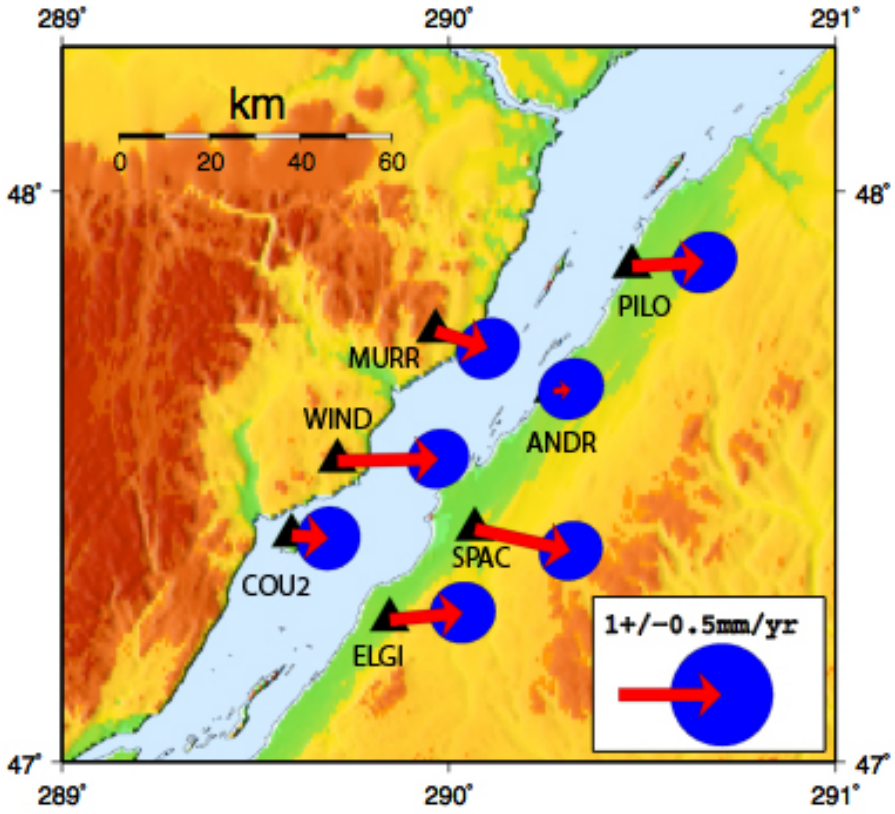

Figure 5.3: Horizontal velocities mapped into the stable NOAM of ITRF2000 at the 1σ confidence interval

SITE	V_E (mm/yr)	V_N (mm/yr)	V_{HOR} (mm/yr)	σ_E (mm/yr)	σ_N (mm/yr)	Correlation
ANDR	0.17	0.02	0.17	0.32	0.30	0.11
COU2	0.36	-0.03	0.36	0.31	0.31	0.05
ELGI	0.71	0.07	0.71	0.32	0.30	0.04
MURR	0.51	-0.17	0.54	0.31	0.30	0.12
PILO	0.70	0.04	0.70	0.32	0.30	0.14
SPAC	0.93	-0.21	0.95	0.31	0.29	0.09
WIND	0.98	0.02	0.98	0.30	0.29	0.09

Table 5.3: Horizontal velocities of Charlevoix sites on the stable NOAM at the 1σ confidence interval

activity could be more thoroughly detected [Mazzotti et al. (2005)]. The uncertainties in the site velocities would be significantly reduced compared to what is currently available with only two episodic campaigns that contain only a few days of data each.

What is most noticeable is the coherent pattern of drift in the east direction of about 0.6 mm/yr.

5.2.5 Vertical velocities of Charlevoix sites

Figure 5.4 shows the vertical velocities for the Charlevoix sites with associated error ellipses. It is important to point out that the error ellipse is uni-dimensional, but for the sake of representation and later comparisons a circle is utilized (with both axes having the same standard deviation). Table 5.4 shows the values of these site velocities and standard deviations.

SITE	V_U (mm/yr)	σ_U (mm/yr)
ANDR	4.2	1.4
COU2	3.9	1.4
ELGI	3.0	1.5
MURR	4.0	1.4
PILO	3.7	1.4
SPAC	4.2	1.3
WIND	4.4	1.3

Table 5.4: Vertical velocities of Charlevoix sites from GPS at the 1σ confidence level

As previously mentioned, the NOAM rotation pole does not account for vertical motion of the crust, and are therefore not mapped into the stable NOAM plate.

The vertical component of the velocity vector varies between 3.0 mm/yr and 4.4 mm/yr, the lowest being ELGI with a standard deviation of 1.5 mm/yr and the highest being ANDR at 1.4 mm/yr. The overall average velocity is 3.9 mm/yr, where the average on the south shore is 3.7 mm/yr and the north shore of 4.2 mm/yr, a 0.5 mm/yr difference. The vertical velocities are spatially coherent relative to each other,

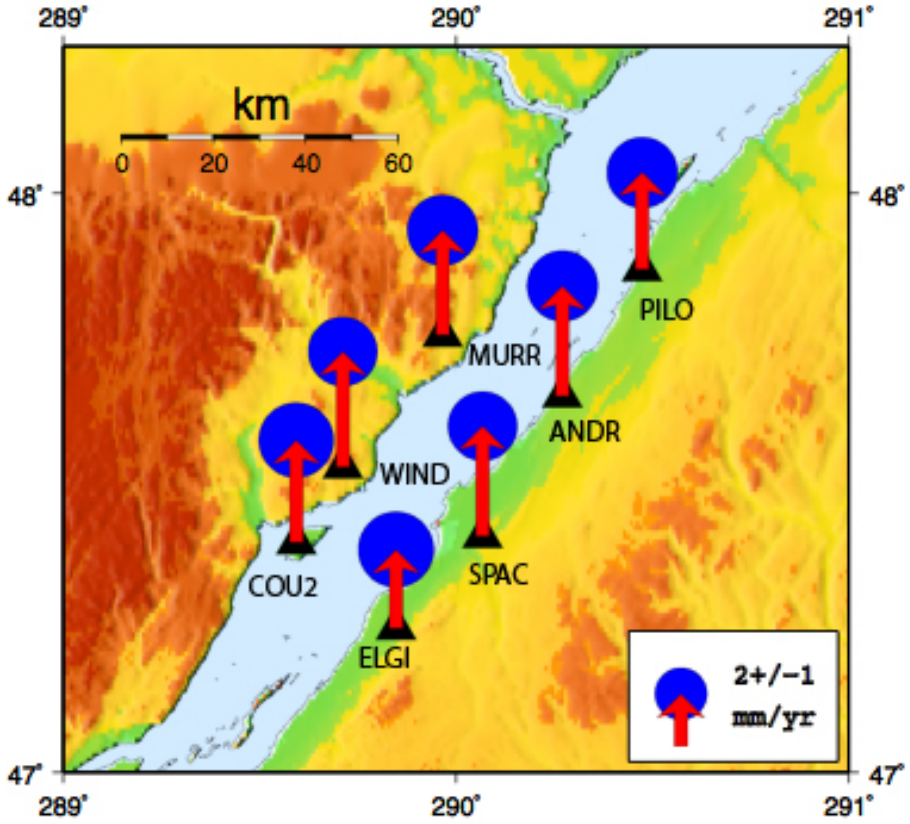

Figure 5.4: Vertical velocities of Charlevoix sites from GPS

and as will be shown in chapter 6, coherent with previous GPS campaigns results and postglacial rebound models.

Chapter 6

Comparison and validation of results

This chapter will focus on the comparison of the horizontal and vertical deformations from GPS of chapter 5 with the results from previous GPS campaigns in eastern Quebec, and postglacial rebound models. The relative velocities of repeating levelling lines outside the CSZ from chapter 3 are also compared with the vertical deformations from both the previous GPS campaigns in eastern Quebec and a PGR model.

6.1 Eastern Canada CBN results

In the following section, the previous GPS campaigns that involve the CSZ will be presented. Then, comparisons will be made between the results obtained in this work with those from that larger network in both the horizontal and vertical components. The levelling results from section 3.6 are also compared with the vertical component of the GPS campaign results and a PGR model.

6.1.1 Previous GPS surveys and their characteristics

A small subset of the CBN consisting of sixteen GPS stations in the seismicity region of the lower Saint Lawrence valley were observed by Stéphane Mazzotti from the Pacific Geoscience Center (PGC) and published in Mazzotti et al. (2005). The monuments typically consisted of concrete pillars with force centering brass plates as a reference point and anchored to bedrock. The stations were surveyed 3 or 4 times between 1994/1996 and 2003 using geodetic dual-frequency GPS receivers and choke ring design antennas for 2 to 7 days per site per survey.

Mazzotti et al. (2005) processed the GPS data with BERNESE, albeit with v4.2. The daily positions were computed using an ionospheric-free, double difference phase solution with precise satellite orbits and Earth rotation parameters from the IGS. The data was sampled at 30 second intervals, the a priori coordinates of the stations were constrained daily according to their nominal ITRF2000 positions and velocities, and the ambiguities were resolved using QIF. Tropospheric delay corrections were also applied using Dry Niell mapping function with 24 zenith delay estimates and 4 gradient parameter estimates per 24-hour session. Changes in antenna models and phase center corrections were accounted for using IGS phase center calibrations. [Mazzotti et al. (2003)]. The three core IGS stations used for fixing the reference were ALGO, STJO, and WES2 (Westford, Massachusetts).

Compared to Tables 4.2 and 4.7, the differences in the processing strategies are minor between the two studies. In 1991, only one tropospheric delay correction per site is estimated due to the short session lengths. Another difference is the choice of reference stations. In the 2005 campaign, WES2 is not used and there were 5 reference stations, as opposed to three. In 1991, as explained in section 4.3.2, only one reference station, ALGO, is used. The impact of this last option was explained in detail in chapter 4.

Most importantly, the velocities which are originally in the ITRF2000 reference frame were also mapped into a stable NOAM reference using the ITRF2000/North America rotation vector (section 5.2.2) defined by Altamimi et al. (2002). As such, the relative horizontal velocities published can be compared with the ones calculated

in section 5.2.4.

6.1.2 Stable North America horizontal velocity comparisons

Figure 6.1 shows the horizontal velocities of the CBN subset of the lower Saint Lawrence river. The CBN sites in the Charlevoix region cannot be directly compared with those from the Charlevoix network because they are not the same markers. But comparisons can be made between the CBN sites and the Charlevoix network sites as a whole.

Compared to Figure 6.2, it can be seen that the drift is in the southeast direction for the CNB sites and the Charlevoix sites are more towards the east. There is good agreement between horizontal velocities for the CBN site velocities and the Charlevoix campaign velocities. The horizontal velocity of LPOC from Mazzotti et al. (2005) (located near site SPAC) has a value of 1.1 mm/yr, which is coherent with the velocities of the Charlevoix sites, which has an average of no greater than 1 mm/yr with a standard deviation of 0.3 mm/yr. The same can be said of the CHRV station (near

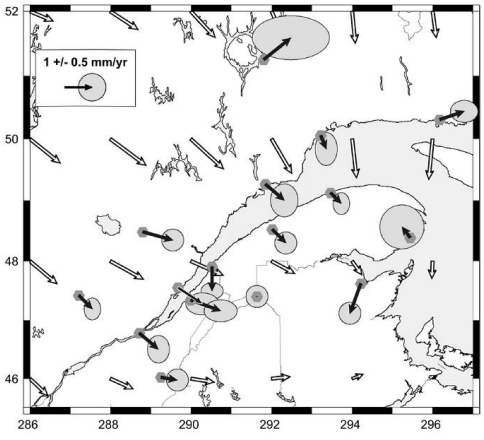

Figure 6.1: Horizontal velocities of CBN sites in eastern Canada with respect to stable NOAM [from Mazzotti et al. (2005)]. Black arrows are GPS campaign results and white arrows are PGR model predictions

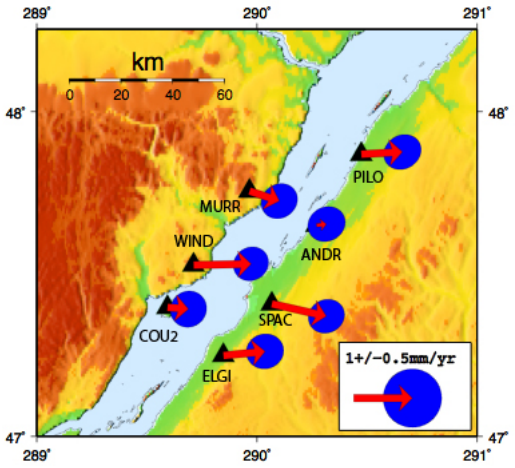

Figure 6.2: Horizontal velocities of Charlevoix sites from 1991 and 2005 campaigns with respect to stable NOAM

WIND) located on the north shore, which has a horizontal velocity of 1.1 mm/yr. The CACO site (located near site PILO)has an irregular behavior compared to the other CBN sites, with a southward drift of 0.9 mm/yr.

6.1.3 Vertical velocity of Charlevoix network comparisons

Charlevoix GPS results

Figure 6.3 shows the vertical velocities of the CBN subset of the lower Saint Lawrence river compared with the velocity results from the Charlevoix campaign vertical velocities. As mentioned above, the CBN sites and Charlevoix network sites cannot be compared directly due to the fact that they are not the same markers.

Once again, compared to Figure 6.4, there is good agreement between the vertical CBN velocities and the Charlevoix campaign velocities as both show an absolute uplift signal. The LPOC vertical velocities from the CBN solution is approximately 2.6 mm/yr with a standard deviation of 0.8 mm/yr, which is comparable to the velocities in Figure 6.4, at an average of between 3 and 4 mm/yr with a standard deviation of around 1.3 mm/yr. The other stations in the CSZ from the CBN solution, CHRV and CACO, both have vertical velocities of around 2.3 mm/yr. Table 6.1 at the end of the chapter shows a summary of these comparisons.

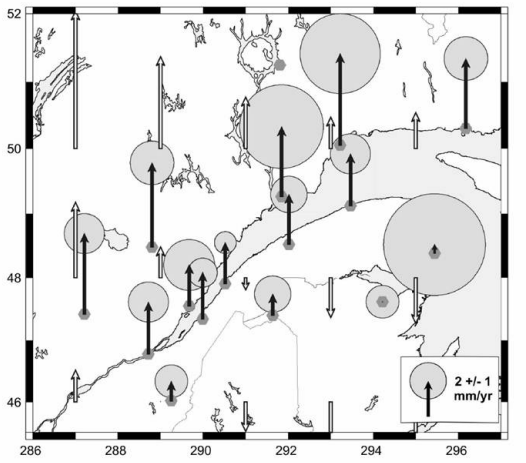

Figure 6.3: Vertical velocities of CBN sites in eastern Canada from Mazzotti et al. (2005). Black arrows are GPS campaign results and white arrows are PGR model predictions

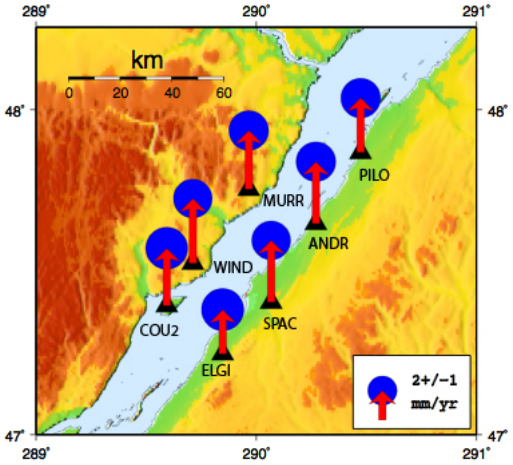

Figure 6.4: Vertical velocities of Charlevoix sites from 1991 and 2005 campaigns

Levelling results

Since the GPS results are tied to the ITRF2000, they are absolute velocities. The velocity results of section 3.6 are only relative since the starting point was set to zero. As such, they are not directly comparable. What is comparable is the difference in vertical velocity between two GPS points that are approximately at the beginning and the end of the levelling lines and the velocity difference from the beginning of the levelling line and that of the end. As such, the difference of the vertical velocities from Figure 6.3 from those found in section 3.6, which are shown in Figure 6.6, can at least show a comparison of the uplift trend. Also, Figure 6.5 is presented once again and represents the levelling lines from Figure 6.6.

Figure 6.5 is the same figure as Figure 3.11, except that it also includes the location of the CBN GPS points from Mazzotti et al. (2005). These are the points used to compare the relative levelling velocity variations (from the linear regression fit) with those from the GPS CBN survey results. The levelling velocities, presented initially in chapter 3 (3.12 to 3.17), are shown in Figure 6.6 and a further analysis follows. Line 001 has a difference in velocity from the beginning of the levellling line to the end

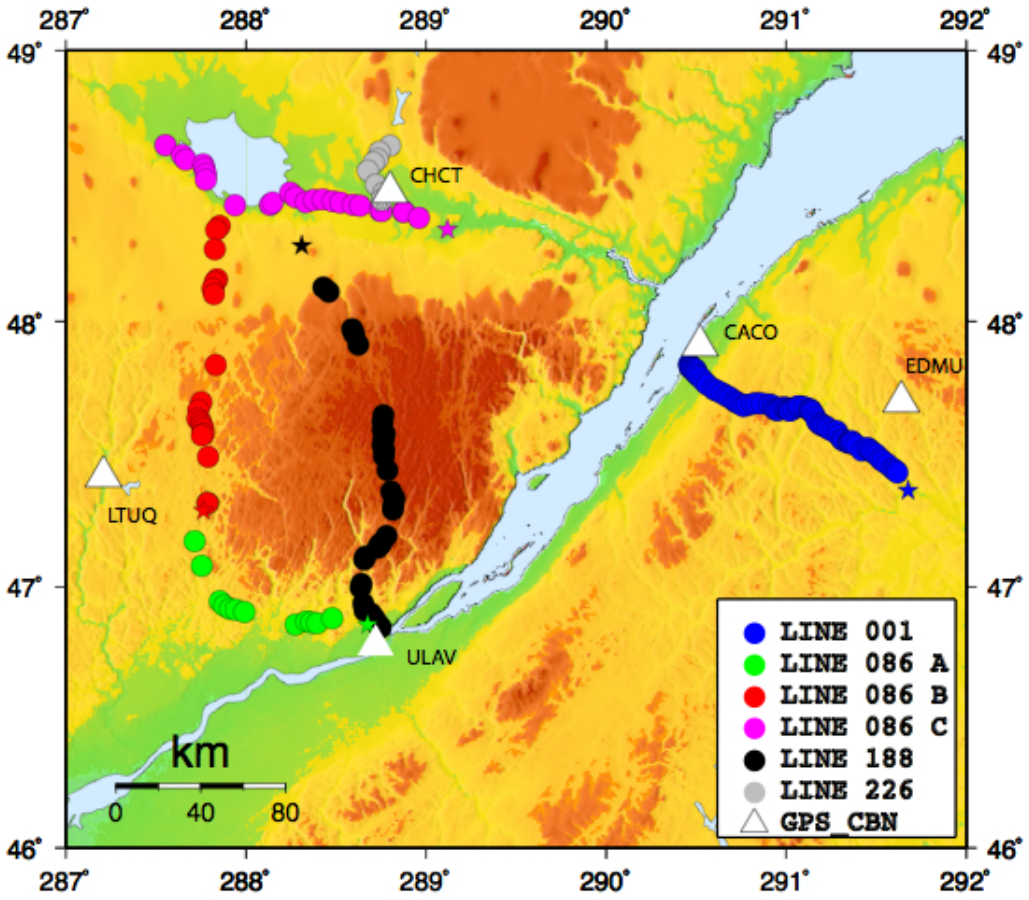

Figure 6.5: Location of levelling lines with multiple common markers outside of CSZ. Stars indicate starting point (relative velocity = 0 mm/yr). CBN GPS sites from Mazzotti et al. (2005) are also presented.

of approximately 7 mm/yr. The GPS CBN results between sites CACO and EDMU show a vertical velocity difference of 1 mm/yr. Line 086A, on the north shore, has an approximate difference from the beginning of the levelling line to the end of about 2 mm/yr. The GPS CBN site velocity difference between sites LTUQ and ULAV is around 2 mm/yr. Approximately the same values can be found for line 086B, which shows a levelling velocity difference of 2 mm/yr to the 1 mm/yr for the GPS CBN sites LTUQ and ULAV once again. Line 086C has a velocity levelling difference of approximately 2 mm/yr compared to the GPS CBN difference of 0 mm/yr of sites LTUQ and CHCT. Line 188 has a levelling velocity difference of 0 mm/yr and the GPS CBN difference between sites ULAV and CHCT is -2 mm/yr. The final line is 226,

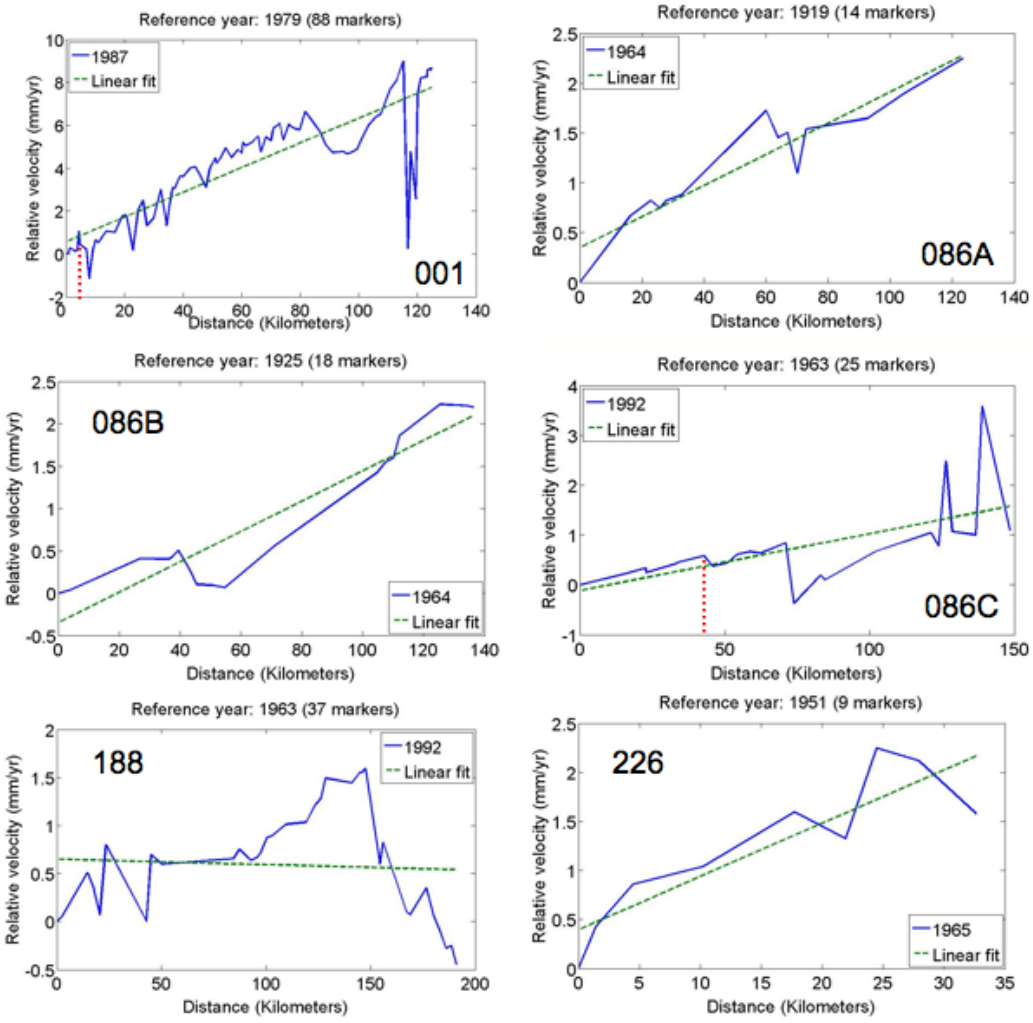

Figure 6.6: Relative velocities of markers from levelling lines illustrated in Figure 6.5

which has a levelling velocity difference of approximately 2 mm/yr. Comparatively, the difference between the GPS CBN sites CHCT and LTUQ is 0 mm/yr. Figure 6.6 shows the two points used to calculate the levelling line uplift difference from the linear regression results. These are represented by the vertical dashed red lines in the velocity graphs of Figure 6.6. If they are not represented, it means that the two points are the first and last markers. Due to the use of the linear fit, these results are only presented at the millimeter level.

So overall, Line 001 on the south shore and lines 086A, 086B, 086C and 226 on the north shore show the same trend of uplift as the absolute velocities by GPS of Figure 6.3, which are the black arrows. This means that the magnitude of uplift is much

greater towards the Lac Saint-Jean area than closer towards the Saint Lawrence river on the north shore and a greater uplift towards the Saint Lawrence river on the south shore than further inland.

On the other hand, line 188 on the north shore does not show any significant uplift trends. The uplift remains constant throughout, or is minimal.

6.2 Postglacial rebound model

In this section, more details will be given about the model constraints of the postglacial rebound simulations conducted at PGC. Following this, a comparison between the results in this research and the model results in both the horizontal and vertical velocity components will be discussed.

6.2.1 Definition and model constraints in eastern Canada

The ICE-3G model is a high resolution global model of late Pleistocene deglaciation inferred on the basis of geophysical predictions of postglacial relative sea level variations in which the ice-ocean-solid Earth interaction is treated in a gravitationally self-consistent fashion. The PGR model velocity vectors are the representation of a lithospheric response to the ICE-3G ice history assuming a spherical compressible Maxwell viscoelastic Earth. The rheology profile used for the calculations consisted of a 120 km thick elastic lithosphere which was used in the development of ICE-3G and termed VM1 [Tushingham and Peltier (1991), Mazzotti et al. (2005)].

6.2.2 Stable North America horizontal velocity comparisons

The PGR horizontal velocities are the white arrows from Figure 6.2. The predicted LPOC site horizontal velocity is 1.1 mm/yr in the southeast direction compared to

the average of 1 mm/yr southeast for the Charlevoix network. As for the CHRV site, the horizontal velocity is around 1.2 mm/yr in the southeast direction. The CACO site, located at the northeast boundary of the CSZ has a predicted horizontal value of 1.0 mm/yr in the southeast direction. It is important to note here as well that we cannot make a direct comparison between the predicted PGR horizontal velocities and the Charlevoix network sites as they are not the same markers, although the ICE-3G model values could have been calculated at these 2005 sites. Only this could have allowed a direct comparison. The same applies for the vertical velocities in section 6.2.3.

6.2.3 Vertical velocity of Charlevoix sites comparisons

Charlevoix GPS results

The pattern of vertical uplift in the Charlevoix region predicted from the PGR models in Figure 6.3 shows a clear line between uplift and subsidence at the Saint Lawrence river. The results from the Charlevoix network do not agree with this prediction. On both the north and south side of the Saint Lawrence river, the Charlevoix network shows an uplift, as shown in Figure 6.4. The predicted LPOC and CACO vertical velocities are -0.2 and -0.3 mm/yr compared to the average Charlevoix network vertical velocity of 3.7 mm/yr. On the north shore, the CHRV site has a vertical uplift predicted velocity of 0.3 mm/yr, compared to the average of 4.1 mm/yr. What can be seen is that the average of uplift is higher on the north shore of the Saint Lawrence than the south shore of the Charlevoix network results, that is an average of 4.1 mm/yr on the north shore and 3.7 mm/yr on the south shore.

Table 6.1 shows a summary of velocity differences between the Charlevoix network, the CBN solutions and the predicted PGR velocities.

Component	site	CSZ network average velocity (mm/yr)	CBN velocity (mm/yr)	PGR model velocity (mm/yr)
Horizontal	LPOC	0.6 E	1.1 SE	1.1 SE
	CACO		0.9 S	1.0 SE
	CHRV		1.1 SE	1.2 SE
Vertical	LPOC	3.9	2.6	-0.2
	CACO		2.3	-0.3
	CHRV		2.3	0.3

Table 6.1: Summary of CSZ GPS horizontal and vertical velocities with GPS CBN solutions and predicted PGR model velocities

Levelling results

The absolute velocities from the PGR models, which are the white arrows from Figure 6.3, cannot be directly compared with the relative velocities from Figure 6.6. But, as in section 6.1.3, what can be compared is the variation in vertical velocity between the PGR predicted sites, which are at the same location as the GPS sites, and the difference in vertical velocity between the beginning of the levelling line and the end from the linear fit line.

Table 6.2 shows that the PGR predicted velocity difference between sites CACO and EDMU is 2 mm/yr and that from the beginning of levelling line 001 and the end is approximately 7 mm/yr. Line 086A and 086B both have the same sites compared, that is LTUQ and ULAV, which shows a velocity difference of 2 mm/yr. Both levelling lines 086A and 086B show a difference in vertical velocity between the beginning and the end of the levelling line of 2 mm/yr. Line 086C shows a difference in velocity from the beginning of the line to the end of approximately 2 mm/yr, compared to the PGR predicted velocity difference of 1 mm/yr between sites LTUQ and CHCT. Line 188 shows an approximate velocity difference of 0 mm/yr between the beginning and the end of the levelling line, whereas the PGR velocity difference is -2 mm/yr between sites ULAV and CHCT. The final line, 226, has a velocity difference of 2 mm/yr, compared to -1 mm/yr for the PGR velocity difference at the CBN GPS sites. The velocity variation for line 001 is much higher than the other values. The fact that it is the only

line analyzed on the south shore and measured more recently (1979 and 1987) than the other lines might give some clues for further investigations.

Overall, on the south shore, line 001 does not show the same subsidence behavior as the PGR model predicted velocities. The PGR model shows an increase in subsidence away from the Saint Lawrence river, and the general uplift trend is increasing towards the river for line 001. On the north shore, lines 086A, 086B, and 086C also show an increase in relative uplift towards the northwest away from the Saint Lawrence river, much like the PGR predicted velocity trend. Lines 188 and 226, on the other hand, do not show the same general uplift trend as the PGR models. The latter is due to the fact that the CBN sites used for comparisons are not optimally placed in relation to the levelling line.

Line	Levelling (mm/yr)	GPS CBN (mm/yr)	PGR CBN (mm/yr)	GPS CBN sites Last - First
001	7	1	2	CACO - EDMU
086A	2	2	2	LTUQ - ULAV
086B	2	1	2	LTUQ - ULAV
086C	2	0	1	LTUQ - CHCT
188	0	-2	-2	ULAV - CHCT
226	2	0	-1	CHCT - LTUQ

Table 6.2: Velocity difference comparison between levelling, GPS CBN results, and PGR model

Chapter 7

Conclusion and future work

This final chapter is composed of two sections. The first outlines the conclusions from the study of the crustal deformation in the CSZ and the second will present some prospectives on future work.

7.1 Conclusion

The objective of this research was to quantify the PGR signal in the CSZ using two precise geodetic methods, levelling and high precision GPS from two campaigns, one in 1991 and the other in 2005. It is then possible to validate the results using previous GPS campaigns executed on CBN pillars in eastern Canada and PGR models derived from postglacial sea-level change on continental deformation.

The relative vertical motion of markers has been derived from independent levelling lines from the first order Canadian network in eastern Canada for the CSZ zone and outlying areas. The relative vertical velocities from section 3.6 show a coherent variation in velocity that increases in amplitude in the northwest direction.

Also, with the use of two high precision GPS campaigns, in 1991 and 2005, the PGR signal was quantified by post processing these observations with the specialized

academic GPS software, BERNESE v5.0. The software enabled us to post process the data with a precision of a few millimeters by taking into account important parameters that influence the accuracy and precision of the coordinate solutions and also to utilize IGS sites and products to tie the CSZ GPS network to the ITRF2000, the realization of the International Terrestrial Reference System for Earth science applications.

For the 2005 campaign, the conventional processing method for obtaining coordinates of sites from high precision GPS observations was employed as described in section 4.1. The 1991 observations, on the other hand, had to be processed using a method in which the internal geometry of the 1991 Charlevoix network is first adjusted, where the fixed ambiguities are obtained using a technique called widelaning (section 4.3.2). Then, using the Quasi Ionosphere-Free (QIF) ambiguity resolution strategy, the inner network is tied to the IGS site ALGO.

The site velocities from the common sites between 1991 and 2005 are then calculated by being introduced as unknown constant parameters in the least squares adjustment, where a priori velocities are obtained from the NUVEL-1A tectonic plate model of Demets et al. (1994). The IGS site, ALGO, is constrained to its nominal position and velocity with a standard deviation of 1 mm and 1 mm/yr, respectively.

The horizontal velocities calculated are obtained in the ITRF2000 frame, which means that the velocities include the motion of the rigid North American (NOAM) Plate. The results are highly correlated with the choice of the rotation vector to map the horizontal velocities originally in the ITRF2000 (section 5.2.1) onto the stable NOAM. In this work, the rotation vector applied is that derived by Altamimi et al. (2002) in order to be able to compare the CSZ results obtained with that from previous GPS campaigns published in Mazzotti et al. (2005).

The results on the stable NOAM plate show that the horizontal velocity agrees well with previous GPS campaigns involving the CSZ, that is an east trend in the general drift pattern on the stable NOAM for the Charlevoix network and a southeast/east drift pattern for the previous GPS campaign. What is less obvious is the significance of the individual horizontal velocities of each site independently. The horizontal velocities are at the limit of GPS resolution for campaign data, which is around 0.5 mm/yr to 1

mm/yr for campaign data over 6-9 years [Mao et al. (1999)]. The horizontal velocities on stable NOAM do not exceed 1 mm/yr, as shown in section 5.2.4, and the average standard deviation at the 1σ confidence interval is around 0.3 mm/yr.

For the vertical velocities of the CSZ sites, the results from section 5.2.5 show an uplift on both sides of the Saint Lawrence river with a higher average on the north shore than the south shore which is comparable to both previous GPS campaigns of Mazzotti et al. (2005) and the VM1 PGR model of Tushingham and Peltier (1991). The average of the velocities of the 3 sites on the south shore of the Saint Lawrence is 3.7 mm/yr compared to 4.2 mm/yr on the north shore. However, in our study, since the standard deviation of the vertical values are around 1.4 mm/yr for all the sites, as shown in Figure 5.3, this does not constitute a significant result from a statistical point of view.

The variation in amplitude of the vertical velocities from the levelling lines compared to the difference in vertical velocities from GPS and predicted PGR velocities show a comparable trend in the uplift gradient towards the northwest in eastern Canada. The GPS CBN results and PGR prediction results shows variations in the absolute vertical velocities of 2 mm/yr between the Saint Lawrence river and Lac Saint-Jean, which is comparable to the relative 1 to 2 mm/yr obtained from the levelling velocity differences.

7.2 Future work

In Stein (2007), Newman (2007), and Rydelek (2007), there is ongoing debate as to the validity of the assessment of earthquake hazard in the New Madrid seismic zone (NMSZ), located in the central United States, which is an intraplate environment with high seismic activity much like the CSZ. The issue is based on whether or not the small motions inferred from geodetic measurements are actually the result of strain accumulation that will eventually be released by large earthquakes and if models of high seismic hazard in the region are supported by the geodetic data and historic earthquake data.

As illustrated above, the CSZ horizontal velocities are at the limit of GPS resolution. It would be interesting to derive the strain rate tensors across the GPS network from the horizontal and vertical velocities on stable North America in order to compare them with the strain rates defined by the seismic catalogue, the CBN GPS measurements, and PGR models in both amplitude and direction as done with the CBN GPS velocities in Mazzotti et al. (2005). Such studies could also be used in the determination of whether or not the motions derived from geodetic measurements are indeed statistically significant in assessing whether or not the strain accumulation would eventually be released by large earthquakes. Adding more permanent GPS stations in the CSZ would also allow for better site velocity resolution, which would increase the accuracy of the strain rate tensors derived.

The limited spatial coverage in the CSZ and other intraplate environments play as much of a role in the interpretation of the horizontal and vertical velocities as the resolution of the GPS observations themselves. The installation of permanent stations with continuously running GPS receivers would decrease significantly the uncertainties in both the horizontal and vertical site velocities. Short term variations in the velocities could be detected. As well, seasonal signals and potential offsets could be estimated to reduce the overall error in the estimated velocities.

Also, absolute gravimetry (AG), which is independent of GPS, has demonstrated that it plays a complimentary role to GPS, especially while monitoring vertical motions. Repeated GPS and AG observations at collocated sites can provide insight into the geophysical processes that drive the observed deformation because AG is sensitive not only to deformation alone, but also to internal mass changes [Henton et al. (2006)]. This would be especially useful in the CSZ because of the fact that the PGR driven crustal deformation, especially in the horizontal direction, is at the limit of GPS resolution. Cooperations with working groups in AG could be established for future GPS campaigns. The observations could be used to obtain more information on the motion.

The PGC, in cooperation with the CRG, have plans to measure the 2005 Charlevoix network again every couple of years for the next 10 years. There are also plans to possibly install more permanent GPS stations in the CSZ to complement the already existing permanent GPS station LPOC. It will be possible to use the observations

collected from bi-yearly GPS campaigns and continuous GPS stations to resolve the short-term (less than one year) deformation episodes. This will allow for better time and spatial resolution than currently available with only the 1991 and 2005 campaign GPS data. Still, it was possible to extract velocities of site positions with a precision of a few millimeters per year with two GPS campaigns, one of which was during the pre IGS era.

Bibliography

Altamimi, Z., Sillard, P., and Boucher, C. (2002). ITRF2000: A new release of the International Terrestrial Reference Frame for earth science applications. *Journal of Geophysical Research*, 107(B10):2214–2233.

Berube, M. (1989). *Étude du mouvement de la croûte terrestre dans la région de Charlevoix*. Levés géodésiques du Canada, Ottawa. 48pp.

Buchbinder, G., Lambert, A., Kurtz, R., Bower, D., Anglin, F., and Peters, J. (1988). Twelve years of geophysical research in the Charlevoix seismic zone. *Tectonophysics*, 156:193–224.

Demets, C., Gordon, R., Argus, D., and Stein, S. (1994). Effect of recent revisions to the geomagnetic reversal time scale on estimates of current plate motions. *Geophysical Research Letters*, 21:2191–2194.

Henton, J., Craymer, M., Dragert, H., Mazzotti, S., Ferland, R., and Forbes, D. (2006). Crustal motion and deformation monitoring of the Canadian landmass. *Geomatica*, 60(2):173–191.

Herring, T., King, R., and McClusky, S. (2006). *GAMIT Reference Manual*. Massachussetts Institute of Technology, Massachussetts. 182pp.

Hoffmann-Wellenhof, B. and Moritz, H. (2005). *Physical Geodesy (2^{nd} Edition)*. SpringerWien, New York. 403pp.

Hugentobler, U., Dach, R., Fridez, P., and Meindt, M. (2004). *Bernese GPS software version 5.0*. Astronomical Institute, University of Bern, Bern. 574pp.

Kenner, S. and Segall, P. (2000). A mechanical model for intraplate earthquakes: Application to the new Madrid seismic zone. *Science*, 289:2329–2332.

Kouba, J. and Héroux, P. (2001). Precise Point Positioning using IGS orbit and clock products. *GPS Solutions*, 5(2):12–28.

Kreyszig, E. (1979). *Advanced engineering mathematics (4^{th} Edition)*. John Wiley and Sons, New York. 939pp.

Lemieux, Y., Tremblay, A., and Lavoie, D. (2003). Structural analysis of supracrustal faults in the Charlevoix area, Quebec: Relation to impact cratering and the St-Laurent fault system. *Canadian Journal of Earth Sciences*, 40:221–235.

Mao, A., Harrison, C., and Dixon, T. (1999). Noise in GPS coordinate time series. *Journal of Geophysical Research*, 104(B2):2797–2816.

Mazzotti, S., Dragert, H., Henton, J., Schmidt, J., Hyndman, R., James, T., Lu, Y., and Craymer, M. (2003). Current tectonics of northern Cascadia from a decade of GPS measurements. *Journal of Geophysical Research*, 108(B12):2554–2572.

Mazzotti, S., James, T., Henton, J., and Adams, J. (2005). GPS crustal strain, post-glacial rebound, and seismic hazard in eastern North America: The St Lawrence valley example. *Journal of Geophysical Research*, 110(B11):301–317.

McCarthy, D. and Petit, G. (2004). *IERS Conventions (2003)*. Bundesamt fur Kartographie und Geodäsie, Franfkurt am Main. 127pp.

Meyer, T., Roman, D., and Zilkoski, D. (2006). What Does Height Really Mean? Part III: Height Systems. *Surveying and Land Information Science*, 66(2):149–160.

Newman, A. (2007). Earthquake risk from strain rates on slipping faults. *Eos (AGU)*, 88:60.

Niell, A. (1996). Global mapping functions for the atmosphere delay at radio wavelengths. *Journal of Geophysical Research*, 101(B2):3227–3246.

Peltier, R. (1994). Ice age paleotopography. *Science*, 265(5169):195–201.

Ray, R. D. (1999). *A global ocean tide model from TOPEX/POSEIDON altimetry: GOT99.2*. NASA Technical Memorandum 209478, Goddard Space Flight Center, Greenbelt, MD. 86pp.

Rondot, J. (1968). Nouvel impact météoritique fossile? La structure semi-circulaire de Charlevoix. *Canadian Journal of Earth Sciences*, 5:1305–1317.

Rydelek, P. (2007). New Madrid strain and postseismic transients. *Eos (AGU)*, 88:60–61.

Santerre, R. (1991). Impact of GPS satellite sky distribution. *Manuscripta Geodetica*, 16:28–53.

Santerre, R. and Beutler, G. (1993). A proposed GPS method with multi-antennae and single receiver. *Bulletin Géodésique*, 67:210–223.

Stein, S. (2007). New Madrid GPS: Much ado about nothing? *Eos (AGU)*, 88:59.

Tushingham, A. and Peltier, W. (1991). ICE-3G: A new global model of late Pleistocene deglaciation based upon geophysical predictions of postglacial relative sea-level change. *Journal of Geophysical Research*, 96(B3):4497–4523.

Véronneau, M., Duval, R., and Huang, J. (2006). A gravimetric geoid model as a vertical datum in Canada. *Geomatica*, 60(2):165–172.

Appendix A

GPS data collection and processing

Presented in this appendix are tables pertaining to the GPS data collection and processing, including the data collected in 1991 and 2005 but not processed because the session was not 24 hours long or because the sites were not observed during one of the campaigns. Intermediate results of the ambiguity resolution in 2005 are also presented.

A.1 2005 GPS data

Table A.1 contains the collected data of the 2005 GPS campaign first presented in section 4.1 not processed. This is due to the fact that either the sites were not observed during the 1991 campaign (newly installed markers) or because the session was not 24 hours long.

Station name	DOY	Observation period (UTC)		
		Start	End	Duration (hrs)
ANDR	201	20:55:00	23:59:30	3.08
CACO	202	18:51:00	23:59:30	5.14
	203	00:00:00	23:59:30	24
	204	00:00:00	12:27:30	12.46
CHRV	207	21:34:00	23:59:30	2.43

Station name	DOY	Observation period (UTC)		
		Start	End	Duration (hrs)
	208	00:00:00	23:59:30	24
	209	00:00:00	16:27:30	16.46
COU2	204	22:24:00	23:59:30	1.59
ELGI	204	20:14:00	23:59:30	3.76
	207	00:00:00	14:18:30	14.31
ESCO	204	14:41:30	23:59:30	9.3
	205	00:00:00	23:59:30	24
	206	00:00:00	23:59:30	24
	207	00:00:00	11:08:00	11.13
HAHA	206	19:37:00	23:59:30	4.38
	207	00:00:00	23:59:30	24
	208	00:00:00	23:59:30	24
	209	00:00:00	19:04:30	19.08
LAUR	201	22:21:00	23:59:30	1.64
	202	00:00:00	23:59:30	24
	203	00:00:00	23:59:30	24
	204	00:00:00	00:21:00	0.35
LOUI	208	00:05:30	23:59:30	23..9
	209	00:00:00	23:59:30	24
	210	00:00:00	12:49:00	12.82
MURR	201	15:49:00	23:59:30	8.18
	204	00:00:00	16:06:00	16.1
PILO	201	17:25:30	23:59:30	6.57
	204	00:00:00	15:10:00	15.17
PSAG	207	18:54:30	23:59:30	5.08
	208	00:00:00	23:59:30	24
	209	00:00:00	23:59:30	24
	210	00:00:00	01:47:30	1.79
SPAC	201	17:21:00	23:59:30	6.64
	204	00:00:00	16:53:30	16.89
SPAM	207	17:00:00	23:59:30	6.99
	208	00:00:00	23:59:30	24

Station name	DOY	Observation period (UTC)		
		Start	End	Duration (hrs)
	209	00:00:00	23:59:30	24
	210	00:00:00	13:41:00	13.68
SRIT	204	12:27:30	23:59:30	11.53
	205	00:00:00	23:59:30	24
	206	00:00:00	23:59:30	24
WIND	204	16:55:00	23:59:30	7.08
	209	00:00:00	14:40:30	14.68

Table A.1: 2005 GPS data characteristics of sessions not processed

A.2 1991 GPS data

Table A.2 contains the collected data of the 1991 GPS campaign first presented in section 4.6 not processed because the sites were not observed during the 2005 campaign.

Station name	DOY	Observation period (UTC)		
		Start	End	Length (hrs)
FOUR	266	13:46:40	19:20:10	5.56
	270	13:36:40	19:04:40	5.47
SERP	263	13:57:40	19:30:00	5.54
	264	13:52:10	19:20:50	5.48
STPA	266	13:39:10	19:11:40	5.54
	270	13:36:10	14:58:40	1.38
TOUR	266	13:45:10	19:10:00	5.41
	270	13:28:40	19:10:00	5.69

Table A.2: 1991 GPS data characteristics of sessions not processed

A.3 Local network site descriptions

Table A.3 lists supplementary characteristics of all the sites from both the 1991 and 2005 campaigns in alphabetical order.

Marker Number	SITE	Site Name	λ, °E	ϕ, °N	h (m)	1991	2005
652013	**ANDR**	**Andréville**	**-69.733**	**47.652**	**163.2**	**x**	**x**
94K0011	CACO	Cacouna	-69.477	47.905	27.31		x
962001	CHRV	Charlevoix	-70.327	47.550	413.4		x
17202	**COUD**	**Ile aux Coudres**	**-70.415**	**47.398**	**63.3**	**x**	
—	**COU2**	**Ile aux Coudres**	**-70.414**	**47.399**	**63.0**		**x**
832004	**ELGI**	**Elgin**	**-70.514**	**47.251**	**100**	**x**	**x**
82K0272	ESCO	Escourt	-69.232	47.467	208.5		x
12204	FOUR	Fournier	-70.146	47.124	628.5	x	
96K1226	HAHA	Lac HA! HA!	-70.778	47.997	486.7		x
90L533	LAUR	Laurentides	-71.209	47.723	741.2		x
—	LOUI	Lac Louis	-69.867	47.977	117.0		x
12200	**MURR**	**Murray**	**-70.042**	**47.756**	**652.5**	**x**	**x**
65K0262	**PILO**	**Pilote**	**-69.521**	**47.869**	**56.9**	**x**	**x**
89KSD41	PSAG	Petit-Saguenay	-70.102	48.201	119.9		x
652014	SERP	Serpent	-69.790	47.993	365.1	x	
652012	**SPAC**	**St-Pacôme**	**-69.919**	**47.410**	**229.7**	**x**	**x**
88KSE85	SPAM	St-Pamphile	-69.769	46.947	340.3		x
96K1231	SRIT	Ste-Rita	-68.955	47.919	274.9		x
652014	STPA	St-Paul	-70.667	47.427	962.2	x	
15200	TOUR	Tourmente	-70.709	47.152	642.6	x	
872001	**WIND**	**Windmill**	**-70.296**	**47.53**	**740.4**	**x**	**x**

Table A.3: Sites of the Charlevoix network for 1991 and 2005 campaigns. In bold are the sites used for this study

A.4 2005 campaign QIF strategy results of ambiguity resolution

Table A.4 contains a more detailed breakdown of the ambiguity resolution success rate presented in section 4.2.2 for the 2005 GPS campaign baselines using the QIF strategy. The 1991 ambiguity results were all presented in detail in chapter 4. All the sites have LPOC as the other station forming the baseline.

DOY	Baseline	Length (km)	L1/L2 resolved	% resolved	$\hat{\sigma}_o$(mm)
202	ALGO	636	86/106	81	1.6
	ANDR	40	94/120	78	1.1
	CAGS	486	84/94	89	1.6
	MURR	46	86/108	80	1.4
	PILO	69	90/124	73	1.2
	SCH2	862	98/152	65	1.4
	SPAC	10	100/120	83	0.9
	STJO	1302	82/110	75	1.5
	UNB1	301	92/130	71	1.4
203	ALGO	636	86/106	81	1.4
	ANDR	40	84/108	78	1.3
	CAGS	486	84/100	84	1.2
	MURR	46	90/118	76	1.5
	PILO	69	88/114	77	1.4
	SCH2	862	94/124	76	1.2
	SPAC	10	96/112	86	1.0
	STJO	1302	82/102	80	1.4
	UNB1	301	90/120	75	1.4
204	ALGO	636	92/100	92	1.1
	CAGS	486	86/100	86	1.2
	SCH2	862	98/114	86	1.1
	STJO	1302	88/98	90	1.3
	UNB1	301	86/128	67	1.4
205	ALGO	636	92/100	92	1.1

DOY	Baseline	Length (km)	L1/L2 resolved	% resolved	$\hat{\sigma}_o$(mm)
	CAGS	486	96/98	98	1.0
	COU2	31	98/110	89	0.9
	ELGI	15	104/114	91	0.8
	SCH2	861	100/118	85	1.0
	STJO	1302	80/98	82	1.4
	UNB1	301	94/118	80	1.1
	WIND	30	98/122	80	1.0
206	ALGO	636	84/98	89	1.5
	CAGS	486	86/98	88	1.5
	COU2	31	92/106	87	1.2
	ELGI	15	98/108	91	0.9
	SCH2	862	94/112	84	1.3
	STJO	1302	80/94	85	1.4
	UNB1	301	90/132	68	1.5
	WIND	30	92/120	77	1.2
207	ALGO	636	82/94	87	1.4
	CAGS	486	82/92	89	1.6
	SCH2	862	84/112	75	1.5
	STJO	1302	78/92	85	1.4
	UNB1	301	88/120	73	1.4
	WIND	30	84/118	71	1.3
208	ALGO	636	88/104	85	1.3
	CAGS	486	88/106	83	1.3
	SCH2	862	88/124	71	1.5
	STJO	1302	78/100	78	1.7
	UNB1	301	92/138	67	1.5
	WIND	30	86/122	71	1.4

Table A.4: Baselines and ambiguity resolution for 2005 campaign

Appendix B

Link of Ile aux Coudres

As discussed in section 4.3.1, the COUD site from 1991 could not be remeasured in 2005 due to the lack of upkeep to the site. Trees had grown around the marker which made the possibility of taking high precision measurements practically impossible without destroying a large majority of the landscape. As such, a new marker was installed approximately 150 meters northeast of the existing COUD site (which was bare of trees) and named COU2 during the July 2005 campaign. This new site was measured for 48 hours. Then on the 1st of November, a link was made between the old COUD point and COU2 using a combination of total station, levelling and GPS surveying methods.

It is important to note that in order to apply the baseline (or eccentricity) between COUD and COU2 in the 1991 post processing, it must be assumed that the vector between the two sites in 1991 and 2005 remains constant. This means that the both markers have not theoretically experienced relative motion to each other.

Figure B.1 shows the network surveyed in 2005. Direct sight using a total station could not be established between COU2 and COUD, and as such a temporary site (COU3) was installed in a clear space so that visibility was possible to both COUD and COU2.

For the total station measurements, two independant tripod installations were done,

and for each, both direct and reverse angles were measured between COUD and COU2 from COU3 with a precision of 3". Four horizontal distances were also measured from COU3 and COU1 with a precision of 1 mm.

The height differences between the three sites derived from spirit levelling were also obtained for all three sites with a precision of 0.4 mm.

A GPS baseline from COU3 to COU2 was measured for a period of 4.75 hours using Ashtech Z-XII receivers and antennas and post processed using GeoGenius by Terrasat, a commercial surveying software. The baseline length, in geocentric coordinates between COU3 and COU2 was obtained with a standard deviation of 1.9, 2.5, and 3.2 mm in the X, Y, Z components, respectively.

Using GEOLAB[1], a network adjustment was done by combining the results from the total station, the geometric levelling and the GPS session while keeping the site COU2 fixed at the a priori values of 1991. These a priori values were obtained by extrapolating the 2005 coordinates of COU2 to 1991 using the NUVEL-1A model described in section 4.3.2.

Figure B.1 shows the relative error ellipses for the three baselines with the error having a scale magnified 1000 times. The values of the relative error ellipses are given in Table B.2.

Table B.1 shows the adjusted site coordinates of the COUD and COU3 sites in ITRF2000, and the fixed coordinates of COU2 extrapolated from fixed 2005 post processing coordinates using NUVEL-1A a priori velocities.

Table B.2 shows the final baseline lengths of the three sites and the relative error values. In bold is the baseline length used to estimate the coordinates of COU2 in 1991 from the COUD observations in section 4.3.2.

The baseline vector components, or eccentricity, between COUD and COU2 is used to estimate the coordinates of COU2 from the observations of COUD.

[1] http://www.msearchcorp.com/Downloads/PDF/GeoLabFieldGuide.pdf

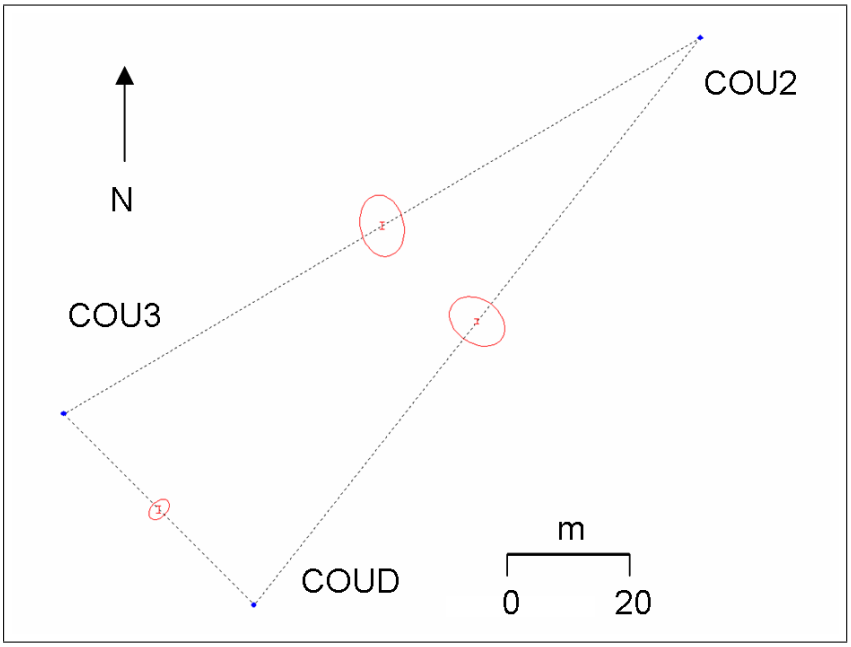

Figure B.1: Relative error ellipses between the three baselines magnified 1000 times

Site	λ, W (dms)	ϕ, N (dms)	h (m)	σ_λ (mm)	σ_ϕ (mm)	σ_h (mm)
COUD	70 24 55.41888	47 23 54.23815	62.9479	2.1	1.8	0.2
COU2	70 24 51.50362	47 23 57.60405	62.9848	0.0	0.0	0.0
COU3	70 24 57.08728	47 23 55.37252	62.2364	1.7	2.3	0.3

Table B.1: Coordinates of Ile aux Coudres sites. Adjusted coordinates for COUD and COU3, and fixed coordinates for COU2 in ITRF2000

From	To	Δ_X (m)	Δ_Y (m)	Δ_Z (m)	a (mm)	Az (°)	b (mm)	σ_h (mm)
COU2	**COUD**	**51.7094**	**99.5859**	**70.3899**	**5.5**	**168**	**4.0**	**0.5**
COU3	COU2	93.7026	85.9260	47.9361	5.7	123	4.0	0.7
COUD	COU3	41.9932	13.6599	22.4538	2.3	45	1.4	0.7

Table B.2: Baseline components and relative station confidence regions at the 95% confidence level for Ile aux Coudres network. In bold are the vector components (or eccentricity) used to estimate the COU2 coordinates from the COUD observations in 1991